

Estimating Population Average Causal Effects in the Presence of Non-Overlap: A Bayesian Approach

Rachel C. Nethery¹, Fabrizia Mealli², and Francesca Dominici¹

¹Department of Biostatistics, Harvard T.H. Chan School of Public Health, Boston MA, USA

²Department of Statistics, Informatics, Applications, University of Florence, Florence, Italy

Abstract

Most causal inference studies rely on the assumption of positivity, or overlap, to identify population or sample average causal effects. When this assumption is violated, these estimands are unidentifiable without some degree of reliance on model specifications, due to poor data support. Existing methods to address non-overlap, such as trimming or down-weighting data in regions of poor data support, all suffer from the limitation of changing the estimand so that inference cannot be made on the sample or the underlying population. This change in estimand may diminish the impact of the study results, particularly for studies intended to influence policy, because estimates may not be representative of effects in the population of interest to policymakers. Researchers may be willing to make additional, minimal modeling assumptions in order to preserve the ability to estimate population average causal effects. We seek to make two contributions on this topic. First, we propose systematic definitions of propensity score overlap and non-overlap regions, which are missing from the existing literature. Second, we develop a novel Bayesian framework to estimate population average causal effects with nominal model dependence and appropriately large uncertainties in the presence of non-overlap and causal effect heterogeneity. In this approach, the tasks of estimating causal effects in the overlap and non-overlap regions are delegated to two distinct models, suited to the degree of data support in each region. Tree ensembles are selected to non-parametrically estimate individual causal effects in the overlap region, where the data can speak for themselves. In the non-overlap region, where insufficient data support means reliance on model specification is necessary, individual causal effects are estimated by extrapolating trends from the overlap region via a spline model. The promising performance of our method is demonstrated in simulations. Finally, we utilize our method to perform a novel investigation of the causal effect of natural gas compressor station exposure on cancer outcomes. Code to implement the method and reproduce all simulations, as well as the data and code to reproduce the natural gas analysis, is available on Github (<https://github.com/rachelnethery/overlap>).

Keywords: Positivity; Overlap; Bayesian Additive Regression Trees; Splines; Natural Gas; Cancer Mortality.

1 Introduction

While the potential to evaluate the causal effects of treatments in randomized studies has long been acknowledged (Fisher, 1935), the development of statistical methods to perform causal inference in observational studies largely began following the seminal work of Rubin (1974). Rubin's work introduced Neyman's potential outcomes framework for causal inference (Neyman, 1923) in the context of observational studies, and he showed that the inherent virtues of randomized studies that allow for simple estimation of causal effects can be artificially imposed on observational data as well. Although great strides have been made in causal inference methods since that time, most

existing methods are developed for idealized observational settings where nearly complete overlap in the confounder distribution across treatments is observed and where causal effects are homogeneous across population sub-groups. In many application areas, these assumptions will not be met, in which case existing causal inference methods yield badly biased estimates of population average causal effects.

In this paper, we seek to make two contributions to the causal inference literature, in the context of the potential outcomes framework. First, we formulate formal definitions of sample propensity score overlap and non-overlap regions. Second, we propose a novel approach to estimating population and sample average causal effects in the presence of non-overlap. Using this approach, the sample is split into a region of overlap (RO) and a region of non-overlap (RN) and distinct models, appropriate for the amount of data support in each region, are applied to estimate the causal effects in the two regions separately. In particular, a Bayesian model is constructed that a) leverages the non-parametric flexibility and predictive accuracy of tree ensembles to estimate causal effects in the RO; and b) relies on splines to extrapolate trends in the causal effect surface into the RN. This approach limits the dependence of average causal effect estimates on model specification by using a non-parametric method where strong data support exists and performs principled model-based extrapolation where insufficient data support is available. In a wide variety of simulated data structures exhibiting propensity score non-overlap and non-linear, heterogeneous causal effects, we have found that the proposed approach leads to improved estimation of the population average causal effects compared to existing methods.

1.1 Causal Inference Notation and Assumptions

We first introduce notation that will be used throughout this article. For subject i , ($i = 1, \dots, N$), Y_i^{obs} will denote the observed outcome (here it will be assumed to be a continuous random variable, in Section 2.4 we introduce analogous notation for the binary outcomes setting), E_i will denote a binary treatment or exposure, and \mathbf{X}_i will denote a vector of observed confounders. Under the stable unit treatment value assumption (Rubin, 1980), potential outcomes $Y_i(1)$ and $Y_i(0)$, corresponding to the outcome that would be observed under scenarios $E_i = 1$ and $E_i = 0$, respectively, exist for each subject $i = 1, \dots, N$. Only one of these potential outcomes is observed, such that $Y_i^{obs} = E_i Y_i(1) + (1 - E_i) Y_i(0)$. An individual causal effect refers to the difference in potential outcomes for an individual, i.e., $\Delta_i = Y_i(1) - Y_i(0)$. The sample average causal effect, sometimes called the conditional average causal effect, is $\Delta_S = E[Y(1) - Y(0)|\mathbf{X}] = \frac{1}{N} \sum_{i=1}^N \Delta_i$, and the population average causal effect, which is the estimand of interest in nearly all causal inference analyses, is defined as $\Delta_P = E_{\mathbf{X}}[E[Y(1) - Y(0)|\mathbf{X}]] = E_{\mathbf{X}}[\Delta_S]$.

The identifiability of sample or population level causal effects in observational studies typically relies upon the assumptions of (1) unconfoundedness and (2) positivity. Unconfoundedness implies that all confounders of the relationship between exposure and outcome are observed, i.e., $(Y_i(1), Y_i(0)) \perp\!\!\!\perp E_i | \mathbf{X}_i$. Throughout this paper we will assume that unconfoundedness holds. Positivity, often stated mathematically as $0 < P(E_i = 1 | \mathbf{X}_i) < 1$, is the assumption that each individual has positive probability of receiving exposure (and therefore also of receiving no exposure). This can also be described as the assumption of sufficient exposure variability across \mathbf{X} or the assumption of “overlap” of the empirical distribution of the measured confounders across the exposure groups. Non-overlap would occur, for example, if people exposed to high levels of an environmental agent $E_i = 1$ are all of low socio-economic status (SES), and SES is a confounder of the relationship between the exposure and health outcome. In such a case, any attempt to adjust for SES when estimating the population average causal effect must rely entirely upon model-based extrapolation, because we have no data that can be used to infer about the potential outcome $Y_i(0)$ for people

of low SES. Thus, in the absence of overlap, the identification of population-level causal estimates requires extrapolation (King and Zeng, 2005). The development of a method that employs minimal and principled extrapolation to estimate population-average causal effects in the presence of positivity violations is the primary focus of our work here.

1.2 Confounder and Propensity Score Non-Overlap

Petersen et al. (2012) discuss settings in which positivity violations, which we also refer to as non-overlap, may arise. We will seek to address only “random” positivity violations, which occur when any individual in the population is, indeed, eligible to receive either of the exposures being compared, but, due to sample limitations, only individuals from a single exposure group were observed in some confounder strata (Westreich and Cole, 2010). For a thorough discussion of “deterministic” positivity violations, i.e., the setting in which some subgroups of the population never receive one of the exposures, see D’Amour et al. (2017), Cole and Hernn (2008), or Westreich and Cole (2010). Petersen et al. (2012) also provide a detailed investigation of how positivity violations can impact each of several classic causal effect estimators, with all of the estimators suffering from bias and increased variance unless they are able to rely on additional assumptions of correct model specification. King and Zeng (2005) discuss at length the bias that can be induced by extrapolating outside the region of common support. Moreover, while the assumption of unconfoundedness becomes more plausible as the number of covariates adjusted for grows, the likelihood of non-overlap increases (Cole and Hernn, 2008; D’Amour et al., 2017); thus, this issue is ever more troublesome in our modern era of high dimensional data.

Random non-overlap in a single confounder can be diagnosed in the observed sample by simply comparing the empirical distribution of that confounder between the exposure groups. However, in practice, multiple hypothesized confounders are typically present, in which case overlap is defined as the presence of both exposed and unexposed subjects in each stratum of the joint distribution of the counfounders (Westreich and Cole, 2010). King and Zeng (2005) proposed using the “convex hull” of the data to define the RO and RN in this context; however, this definition is extremely conservative, as noted by the authors themselves, and cannot be easily generalized or adapted to the needs of a specific method, due to the complexity of the linear programming procedure required to implement it. Thus, in multi-confounder scenarios, overlap is typically evaluated indirectly, by visually assessing overlap in the estimated propensity score (Rosenbaum and Rubin, 1983; Austin, 2011), $\hat{\xi}_i = \hat{P}(E_i = 1 \mid \mathbf{X})$.

To make our approach as general as possible, in this paper we address the issue of propensity score non-overlap. Despite ample literature addressing propensity score non-overlap, no systematic definition of the RO and RN exists, besides the one proposed by Crump et al. (2009), which is motivated by the desire for a minimum variance estimator and may not generalize well to other contexts. Most papers on the topic imply that users can “eyeball” histograms or summary statistics of the propensity score to subjectively define these regions. Thus, one of the primary contributions of this paper will be the introduction of formal and general definitions of the propensity score RO and RN.

1.3 Existing Methods for Estimating Causal Effects in the Presence of Non-Overlap

Methodological proposals for reducing the bias and variance of causal effect estimates in the presence of propensity score non-overlap are abundant in the causal inference literature (Cole and Hernn, 2008; Crump et al., 2009; Petersen et al., 2012; Li et al., 2017); however, to our knowledge,

all of the existing methods suffer from a common limitation— they modify the estimand so that neither sample nor population average causal effect estimates can be obtained. In the environmental health applications of primary interest to us, causal inference analyses are often intended to influence nationwide regulatory policies. In such settings, these modified causal estimands might not be accepted by policy makers to inform regulations because they are not representative of the population under study. Examples of such applications include the effect of power plant emissions on cardiovascular and respiratory-related hospitalizations (Zigler et al., 2016), the effect of unconventional natural gas extraction on childhood cancer incidence (McKenzie et al., 2017a), and the effect of gestational chemical exposures on birth outcomes (Ferguson et al., 2014).

By far the most commonly recommended approach for handling propensity score non-overlap is “trimming” or discarding observations in regions of poor data support (Ho et al., 2007; Petersen et al., 2012; Gutman and Rubin, 2015). Although relatively few papers provide guidance on how to determine which observations should be trimmed, a number of specific suggestions have been made, most in the context of matching (Cochran and Rubin, 1973; LaLonde, 1986; Dehejia and Wahba, 1999; Ho et al., 2007). A summary of the literature on this topic is provided by Crump et al. (2006). An appealing feature of trimming is its flexibility— it can be applied in conjunction with any causal estimation procedure, i.e., matching, weighting, or regression adjustment. However, trimming allows only for the estimation of the average causal effect *in the trimmed sample*, which has a less appealing interpretation in most settings. Moreover, as discussed by Yang and Ding (2018), trimming changes the asymptotic properties of estimator in ways that are often overlooked. Finally, trimming throws away data that may have been expensive or otherwise difficult to obtain and that could provide valuable information about exposure effects. Crump et al. (2009) proposed a procedure that identifies a target sub-population for which an average treatment effect can be estimated with the greatest precision given the overlap in the sample, and the sample is trimmed in accordance with this sub-population. While providing a more systematic approach to trimming and yielding an efficient estimate, the interpretation of the estimand is equally unappealing in many contexts.

A push for more interpretable estimands in the context of non-overlap has motivated several recent methodological developments in the context of weighting approaches to causal inference. These methods also allow all of the data in the sample to be retained for estimation. Li et al. (2017) introduce overlap weights, which weight each member of the sample proportional to its probability of inclusion in its counterfactual exposure group, and they show that these weights result in minimum (asymptotic) variance estimators and yield exact finite sample balance in the means of all covariates across exposure groups. The estimand corresponding to the overlap weights is what Li et al. call the “average exposure effect for the overlap population”, and they claim that the overlap population, the sub-population that contains substantial proportions of both exposed and unexposed individuals, is of interest in many clinical and policy settings. Zigler and Cefalu (2017) implement a similar overlap weighting approach in a Bayesian framework. Yang and Ding (2018) recently introduced a weighting approach that approximates the trimming method of Crump et al. (2009) but is shown to have improved asymptotic properties.

To our knowledge, every existing method proposed in response to propensity score non-overlap has relied on the removal or down-weighting of data in the RN, preferring to endorse a reliable estimate of a causal effect with a less appealing interpretation rather than an estimate of the causal effect in the target population that could contain bias. We are of the opinion that too little emphasis has been placed on the development of methods that (1) minimize model dependence where possible and (2) perform model-based extrapolation in a principled manner where necessary in order to produce estimates of the population estimand of interest with small bias and appropriately large uncertainty in the presence of propensity score non-overlap. In this spirit, we propose here a

Bayesian modeling approach, which estimates individual causal effects (Δ_i) in the RO and the RN, separately.

The first stage of this procedure is an imputation step: a Bayesian Additive Regression Tree (BART) (Chipman et al., 2010), is fit to the data in the RO to impute the missing potential outcomes and thereby estimate causal effects Δ_i for observations in the RO. In the second stage, a spline model is fitted to the estimated Δ_i in the RO, leveraging all available information (i.e., estimated propensity score, all covariates, and the observed potential outcome for each individual), to capture trends in the causal effect surface and is then used to extrapolate those trends to estimate Δ_i for observations in the RN.

The most notable feature of this approach is that it does not modify the estimand, so that the sample or population average causal effects of interest are able to be estimated. It naturally accommodates non-overlap in either/both tails of the propensity score distribution. Thanks to the flexibility of both BART and splines, our model can also capture non-linear associations and heterogeneous causal effects. Moreover, the spirit of classic causal inference is preserved in the RO, where adequate data support is available, by utilizing non-parametric BART to estimate causal effects. In the RN, where insufficient data support requires reliance on model specifications, a flexible parametric model, informed by causal effect trends in the RO, is employed to estimate effects. We note that the data in the RN are excluded from both the BART and spline model fitting, so that the models are never influenced by regions of the data with little support. Believing that extensions of trends captured in the RO typically represent our “best guess” at trends in the RN, we estimate individual causal effects in the RN by extrapolating from a spline fit only to data in the RO.

In Section 2, we provide, for the first time, a systematic definition of the propensity score RO and RN, we provide background on the use of tree ensemble methods in causal inference, and we introduce our method, which we call BART+SPL. Simulated data are used in Section 3 to demonstrate how BART+SPL can provide population average causal effect estimates with less bias than existing methods and appropriate variance. We also provide guidance on the degree of non-overlap that can reliably be addressed with this method. In Section 4, our method is applied to investigate whether natural gas compressor station exposure affects county-level thyroid cancer and leukemia mortality rates. Finally, we wrap up with a summary of our findings in Section 5.

2 Methods

2.1 Definition of Overlap and Non-Overlap Regions

Although King and Zeng (2005) proposed the use of the convex hull of the data to define overlap and non-overlap regions as early as 2005, this appears to be an unpopular criteria, likely due to its extreme conservatism. Crump et al. (2009) noted the absence of a systematic definition of the RO in the causal inference literature. While they offer a definition, their goal is to identify a region of the data that will produce a minimum variance average causal effect estimate rather than to provide a general definition of the region where overlap is observed. Their definition may be ideal in the context of trimming in conjunction with non-parametric causal estimators; however, it is unlikely to be appropriate in more general settings. Ironically, BART itself has also been proposed as method for identifying the RN (Hill and Su, 2013). Because BART yields relatively large uncertainties for predicted values of units in regions of poor data support, Hill and Su (2013) suggest trimming observations with posterior uncertainty values greater than some threshold. They provide several options for defining this threshold.

We intend to provide a more general characterization of the RO and RN here. In fact, we

provide two possible methods of defining the RO and the RN. We first introduce what we call the “point-wise overlap” definition, which is most appropriate for use in scenarios where the data in the RN is being trimmed or down-weighted. The second type of overlap, “interval-wise overlap”, gives a more conservative definition of the overlap region (i.e., the overlap region is smaller and the non-overlap region is larger) and is therefore likely to be preferred in settings where the data in the RN is being fully retained and dealt with through alternative measures, as in our proposed method.

We use the estimated propensity scores, $\hat{\xi}_i$, to define the RO, O , and the RN, O^\perp , in the sample. Throughout this section, we assume that the propensity score model has been correctly specified and that the propensity scores are well estimated; however, we demonstrate and discuss the performance of our method under propensity score model misspecification using simulations in Section 3. Let $\hat{\xi}_{(j)}$ denote the j^{th} order statistic of the $\hat{\xi}_i$ and $P = [\hat{\xi}_{(1)}, \hat{\xi}_{(N)}]$ be the subspace of $(0, 1)$ over which the $\hat{\xi}_i$ are observed. Our definitions allow every point in P to be assigned to either O or O^\perp . In each definition, the user must specify two parameters, denoted a and b , which are used to identify O . O^\perp is then defined as the complement of O , relative to P .

The idea behind point-wise overlap is that, if, at a given point in P , more than b units from each exposure group have estimated propensity scores lying within some interval of size a covering that point, then it is included in the region of overlap. To make this notion formal, we first we lay out notation. Let $\phi_{(h)}(e, o)$ denote the h^{th} propensity score order statistic in exposure group e relative to the point o for $o \in P$. For instance, $\phi_{(1)}(e, o)$ represents the minimum propensity score greater than o in group e and $\phi_{(-1)}(e, o)$ represents the maximum propensity score less than o in group e . If there are fewer than h units with propensity scores less than o in group e , we let $\phi_{(-h)}(e, o) = -\infty$. Analogously, if there are fewer than h units with propensity scores greater than o in group e , we let $\phi_{(h)}(e, o) = \infty$. Denote $\phi_{(0)}(e, o) = o$. We also define

$$u(e, o) = \begin{cases} b, & \text{if } o = \hat{\xi}_i \text{ for some } i \text{ with } E_i = e \\ b + 1, & \text{otherwise} \end{cases}$$

Using this notation, we propose the following definition for the point-wise region of overlap:

$$O_{pw} = \{o \in P : |\phi_{(h)}(e, o) - \phi_{(-(u(e,o)-h))}(e, o)| < a \text{ for some } h \in \{0, \dots, u(e, o)\} \text{ for both } e = \{0, 1\}\}$$

The point-wise region of non-overlap is correspondingly defined as $O_{pw}^\perp = P \setminus O_{pw}$.

The value in our point-wise overlap definition is that it may introduce a more systematic and transparent approach to trimming and down-weighting in the literature, as authors need only provide the parameter values a and b that they specified in order for readers to fully understand how the trimmed or down-weighted RN was chosen. However, we note again that trimming and weighting methods for handling non-overlap change the estimand. In those contexts, defining the RO and RN is equivalent to defining the estimand. While the point-wise overlap definition can always be applied in such settings, it is unlikely to provide an interpretable estimand, and therefore may not be appealing in settings where an interpretable estimand is critical. In such cases, other strategies for defining the RO that prioritize the interpretability of the resulting estimand may be preferable (such as limiting the analysis to observations in some meaningful confounder strata of interest).

The intuition behind interval-wise overlap is more complex. It is built upon the notion of intervals between consecutive ordered propensity scores for each exposure group (separately). Consider a point, o , in the range of the propensity score and (1) the interval C containing o formed by consecutive ordered propensity scores for units from exposure group $e = 1$ and (2) the interval D

containing o formed by consecutive ordered propensity scores for units from exposure group $e = 0$. If, for EACH point in C , more than b units from exposure group $e = 1$ have propensity scores lying within some interval of size a containing it and, for EACH point in D , more than b units from exposure group $e = 0$ have propensity scores lying within some interval of size a containing it, then the point o is assigned to the RO. To define interval-wise overlap, we use similar notation as above with $\phi_{(h)}(e, o)$ denoting the h^{th} propensity score order statistic in exposure group e relative to the point o for $o \in P$; however, we make minor changes to the definitions of these relative order statistics at the boundaries (i.e., we no longer have $\phi_{(-h)}(e, o) = -\infty$ if there are fewer than h units with propensity scores less than o in group e and analogously at the upper boundary). If there are exactly k units with propensity scores less than o in group e , we let $\phi_{(-(k+1))}(e, o) = -\infty$ if $\hat{\xi}_{(1)} = \hat{\xi}_i$ for some i with $E_i = e$ and $\phi_{(-(k+1))}(e, o) = \hat{\xi}_{(1)}$ otherwise, and $\phi_{(-(k+l))}(e, o) = -\infty$ for $l > 1$. Analogously, if there are exactly k units with propensity scores greater than o in group e , we let $\phi_{(k+1)}(e, o) = \infty$ if $\hat{\xi}_{(N)} = \hat{\xi}_i$ for some i with $E_i = e$ and $\phi_{(k+1)}(e, o) = \hat{\xi}_{(N)}$ otherwise, and $\phi_{(k+l)}(e, o) = \infty$ for $l > 1$. We also define the following:

$$v(e, o) = \begin{cases} 0, & \text{if } o = \hat{\xi}_i \text{ for some } i \text{ with } E_i = e \\ 1, & \text{otherwise} \end{cases}$$

Then, the interval-wise RO is:

$$O_{iw} = \{o \in P : |\phi_{(h)}(e, o) - \phi_{(-(u(e,o)-h))}(e, o)| < a \text{ for some } h \in \{v(e, o), \dots, b\} \text{ for both } e = \{0, 1\}\}$$

The interval-wise region of non-overlap is correspondingly defined as $O_{iw}^\perp = P \setminus O_{iw}$.

Interval-wise overlap will be used to define the RO and RN for BART+SPL. In Figure 2 in Section A.2 of the Appendix, we provide an illustration of the types of non-overlap that can be captured by this definition, including the most common case of non-overlap in the tails of the propensity score distribution, non-overlap in the interior of the propensity score distribution, and multiple non-overlap intervals. However, BART+SPL is designed to handle exclusively non-overlap in the tails of the propensity score distribution, and extensions to improve estimation of causal effects in the presence of non-overlap in the interior of the propensity score distribution are left for future work.

In Section 3.4, we provide guidance on the choice of a and b when applying BART+SPL. The rich causal inference literature on caliper selection for matching procedures may provide insight on how to make these choices in other settings (Stuart, 2010; Lunt, 2014).

2.2 Tree Ensembles for Causal Inference

Regression trees are a class of non-parametric and semi-parametric machine learning procedures primarily used for prediction in which a model is constructed by recursively partitioning the covariate space. Notable advantages of regression tree methods over other regression modeling techniques are (1) their internal construction of the regression model, eliminating the need for the user to pre-specify the functional form of the association between the response and predictors, (2) their natural incorporation of relevant high order interactions, and (3) their ability to capture complex non-linear associations. Strobl et al. (2009) provide a thorough introduction to regression trees, and Loh (2014) contribute a survey of the major regression tree fitting algorithms.

Tree ensemble methods, such as random forests (Breiman, 2001; Lin and Jeon, 2006; Biau et al., 2008), bagging (Breiman, 1996; Büchmann and Yu, 2002), boosting (Friedman et al., 2000; Friedman, 2001), and BART (Chipman et al., 2010) gained popularity as a more stable and reliable

generalization of regression trees, which often suffer from overfitting, instability, and high variability. BART (Chipman et al., 2010) is highly regarded for its consistently strong performance under the “default” model specifications, reducing its dependence on subjective tuning and time consuming cross validation procedures. Letting j index the J trees in the ensemble ($j = 1, \dots, J$), a BART is a sum of trees model of the form

$$Y = \sum_{j=1}^J g(\mathbf{X}; \mathcal{T}_j, \mathcal{M}_j) + \epsilon, \quad (1)$$

where g is a function that sorts each individual into one of a set of m_j terminal nodes, associated with mean parameters $\mathcal{M}_j = \{\mu_1, \dots, \mu_{m_j}\}$, based on a set of decision rules, \mathcal{T}_j . ϵ is a random error term that is typically assumed to be $N(0, \sigma^2)$ when the outcome is continuous. BART has also been extended to the binary outcome setting through the addition of the probit link function.

A Bayesian backfitting algorithm is utilized to obtain Markov chain Monte Carlo (MCMC) samples from the posterior distribution of the BART parameters. The BART predicted value for a given individual in the sample is computed as the sum of the J estimated mean parameters corresponding to the terminal node to which the individual was assigned in every tree (these sums are averaged across the K posterior samples). Credible intervals can be constructed from the percentiles of the posterior samples. BART’s strong predictive performance has been reported in many contexts (Zhou and Liu, 2008; He et al., 2009; Chipman et al., 2010; Liu et al., 2010; Bonato et al., 2011; Hill, 2011; Huang et al., 2015; Liu et al., 2015; Kindo et al., 2016; Sparapani et al., 2016).

Thanks to its semi-parametric nature, BART adapts easily to the classic causal estimation paradigm. BART was first introduced as a tool for causal inference and joined with the potential outcomes framework by Hill (2011). A BART is fit to the observed data, including an estimated propensity score in the set of predictors, and its strong predictive capacity is exploited for prediction of the missing potential outcome for each individual, Y_i^{mis} . Then individual causal effects can be estimated as

$$\hat{\Delta}_i = \begin{cases} Y_i^{obs} - \hat{Y}_i^{mis}, & \text{if } E_i = 1 \\ \hat{Y}_i^{mis} - Y_i^{obs}, & \text{if } E_i = 0 \end{cases}, \quad (2)$$

in the continuous outcome setting. While the sample average causal effect estimate is simply the average of the estimated individual causal effects ($\hat{\Delta}_S = \frac{1}{N} \sum_{i=1}^N \hat{\Delta}_i$), the estimating the population average causal effect requires additional integration over the predictors ($\Delta_P = E_{\mathbf{X}}[\Delta_S]$), due to the potential (and likely) interactions between treatment and other predictors in the BART. Below, we propose the use of the Bayesian bootstrap to perform this integration.

Despite BART’s highly accurate prediction and causal effect estimation in regions of the data with strong support, its predictions have been shown to sometimes contain greater bias than those of parametric methods and classic causal inference approaches (e.g., weighting and matching) in the presence of non-overlap (Hill, 2011; Hill and Su, 2013). Because the BART model is built entirely on binary cuts of the observed predictors, it is unable to capture trends in the data, which are used by parametric models to reasonably extrapolate into the RN, and therefore extrapolates poorly. Thus, BART’s sensitivity to non-overlap makes it a risky stand-alone causal inference tool for most real datasets.

2.3 BART+SPL

In this section, we describe BART+SPL, our proposed Bayesian approach for estimating causal effects in the presence of propensity score non-overlap. The first stage of the procedure, which we

call the imputation phase, utilizes a BART to impute the missing potential outcomes and estimate individual causal effects in the RO. In the second stage, which we call the smoothing stage, a spline is fit to the BART-estimated individual causal effects in the RO and is invoked to extrapolate the causal effect trends to the individuals in the RN. Our approach for continuous outcomes is described in Sections 2.3.1 and 2.3.2 in the context of a single iteration of a Bayesian MCMC sampler for the sake of clarity, and in Section 2.3.3, we explain how the draws from the sampler can be invoked to estimate average causal effects, individual causal effects, and associated uncertainties. This model can be implemented through the MCMC procedure described in Section A.1 of the Appendix. In Section 2.4, we introduce an extension to binary outcomes. Throughout this section, all references to the RO and RN refer to the interval-wise overlap definition.

2.3.1 Imputation Stage

In the first stage of BART+SPL, we adopt the common practice of treating the unobserved potential outcome for each individual as missing data, and we construct a BART model to impute these missing values for individuals in the RO. As in Section 2.2, we use Y^{obs} to denote the observed potential outcomes, and Y^{mis} to denote the missing potential outcomes. We also introduce the subscript Oq and subscript $O^\perp r$ notation to refer to data from subjects in the RO and RN, respectively, e.g., Y_{Oq}^{obs} is the observed outcome of individual q in the RO and $Y_{O^\perp r}^{mis}$ is the missing potential outcome of individual r in the RN ($q = 1, \dots, Q; r = 1, \dots, R$). Analogously, subscript O and subscript O^\perp refer to vectors/matrices of the values of all individuals in O and O^\perp , respectively.

In this stage, all of our modeling efforts are focused on the data in the RO, for now ignoring the RN entirely. Y_{Oq}^{mis} is first imputed using a BART model of the form

$$Y_{Oq}^{obs} = \sum_{j=1}^J g(E_{Oq}, \hat{\xi}_{Oq}, \mathbf{X}_{Oq}; \mathcal{T}_j, \mathcal{M}_j) + \epsilon_{Oq},$$

where $\epsilon_{Oq} \sim N(0, \sigma_B^2)$. To do so, the Bayesian backfitting algorithm of Chipman et al. (2010) is utilized to collect a sample from the posterior distribution of $\theta = \{\sigma_B^2, \mathcal{T}_j, \mathcal{M}_j; j = 1, \dots, J\}$, $p(\theta|Y_O^{obs})$. An imputed value of Y_O^{mis} , which we denote \tilde{Y}_O^{mis} , is obtained by sampling from its corresponding posterior predictive distribution (ppd), $p(Y_O^{mis}|Y_O^{obs}) = \int p(Y_O^{mis}|Y_O^{obs}, \theta)p(\theta|Y_O^{obs})d\theta$. Finally, a sample of the individual causal effects in O , Δ_O , is constructed as in Equation 2, by plugging in \tilde{Y}_O^{mis} .

2.3.2 Smoothing Stage

In the second stage, a smoothing model is fit to the BART-estimated individual causal effects in the RO, and the model is employed to estimate the individual causal effects in the RN by extrapolating the trends identified in the RO. With this approach, we impose the assumption that any trends in the individual causal effects (as a function of the propensity score and/or the covariates) identified in the RO can be extended into the RN. By modeling the causal effect surface in this stage rather than the separate potential outcome surfaces, we take advantage of the potentially increased smoothness of the causal effects that may occur in practice. Through tuning, we ensure that the variance in the RN is inflated to reflect the high uncertainty in the region, leading to mildly conservative confidence regions in most realistic scenarios.

Assume for now that the RN includes only exposed individuals ($e = 1$). Let $Y_{Oq}^*(1) = Y_{Oq}^{obs}$ if $E_{Oq} = 1$ and $Y_{Oq}^*(1) = \tilde{Y}_{Oq}^{mis}$ otherwise. Let $rcs(z)$ denote a restricted cubic spline basis for z .

Employing the imputed values obtained in the previous stage, we construct the following smoothing stage model:

$$\tilde{\Delta}_{Oq} = \mathbf{W}'\boldsymbol{\beta} + \epsilon_{Oq}, \quad \mathbf{W} = \begin{bmatrix} rcs(\hat{\xi}_{Oq}) \\ rcs(Y_{Oq}^*(1)) \\ \mathbf{X}_{Oq} \end{bmatrix},$$

where $\epsilon_{Oq} \sim N(0, \sigma_S^2 + I(\hat{\xi}_{Oq} \in O^\perp)\tau_{Oq})$. σ_S^2 is the residual variance for all units in the RO and τ_{Oq} is an added variance component only applied to units in the RN. The purpose of τ_{Oq} is to inflate the variance of units with an estimated propensity score in the RN, to adequately reflect the higher uncertainty in regions of little data support. In this model, τ_{Oq} is clearly unidentifiable, as the model is fit using exclusively data in the RO, and it will only come into play when invoking the ppd to predict in the RN. Here, we choose to treat it as a tuning parameter, and below we describe our recommended tuning parameter specification.

We collect a posterior sample of the parameters, $\psi = \{\boldsymbol{\beta}, \sigma_S^2\}$, from this model. Because the motivation for the smoothing stage is to use the smoothed trends from the RO to predict the individual causal effect values in the RN, the sampled parameter values and the smoothing model predictor values for individuals in the RN are summoned to obtain a sample from the ppd of Δ_{O^\perp} , $p(\Delta_{O^\perp} | \Delta_O) = \int p(\Delta_{O^\perp} | \Delta_O, \psi)p(\psi | \Delta_O)d\psi$. The sample is denoted $\tilde{\Delta}_{O^\perp}$. In the case that both exposed and unexposed units fall in the RN, we define $Y_{Oq}^*(0)$ analogously to $Y_{Oq}^*(1)$ and construct a second model, identical to the one above except replacing $rcs(Y_{Oq}^*(1))$ with $rcs(Y_{Oq}^*(0))$. The ppd from the first model is then used to predict individual causal effects for exposed units in the RN and the ppd from the second model is used for unexposed units. We recommend restricted cubic splines in the smoothing model, because they generally demonstrated superior performance when applied to simulated data, however other spline choices may provide improved performance under some conditions.

Our recommended specification of τ_{Oq} is motivated by the aim to have (1) the variance of individual causal effects increase monotonically as the observation's distance from the RO (i.e., region of strong data support) increases and (2) the increase in variance be in proportion to the scale of the data. Thus, the suggested tuning parameter specification is $\tau_{Oq} = (10d_{Oq})r_O$, where $r_O = \text{range}(\tilde{\Delta}_{Oq})$ and d_{Oq} is the distance from the observation's propensity score to the nearest propensity score in the RO. The effect of this tuning parameter is that, for every .1 unit further we go into the RN, the variance of the individual causal effects increases by the range of the causal effects in the RO. While it could lead to somewhat conservative confidence interval coverage in "simple" situations (situation where the trends in the RN are easily predicted from the trends in the RO), we have found in simulations that this choice of tuning parameter consistently provides both reasonably-sized confidence intervals and acceptable coverage.

2.3.3 Estimation and Uncertainty Quantification

We can iterate the two stages described above M times to obtain $\{\Delta_O^{(1)}, \dots, \Delta_O^{(M)}\}$ from the imputation stage and $\{\Delta_{O^\perp}^{(1)}, \dots, \Delta_{O^\perp}^{(M)}\}$ from the smoothing stage (note that we have traded the tilde notation from above for the (m) notation to differentiate the samples from the M iterations). By iterating between the two stages, we are able to account for the uncertainty in the estimation of Δ_O from the first stage and pass it on to the second stage, where Δ_O is used as the outcome. Thus, the uncertainty in the estimate of Δ_{O^\perp} in the second stage reflects the uncertainty both from stage one and stage two.

For an individual in the RO, their individual causal effect, Δ_{Oq} , is estimated as the posterior

mean over the M samples, $\hat{\Delta}_{Oq} = \frac{1}{M} \sum_{m=1}^M \Delta_{Oq}^{(m)}$. Similarly, for an individual in the RN, their individual causal effect, $\Delta_{O\perp r}$, is estimated as $\hat{\Delta}_{O\perp r} = \frac{1}{M} \sum_{m=1}^M \Delta_{O\perp r}^{(m)}$. Credible intervals for the individual causal effects can be obtained by extracting the appropriate percentiles from these M samples. Samples of Δ_S are produced by $\Delta_S^{(m)} = \frac{1}{N} (\sum_{q=1}^Q \Delta_{Oq}^{(m)} + \sum_{r=1}^R \Delta_{O\perp r}^{(m)})$ for $m = 1, \dots, M$, and $\hat{\Delta}_S = \frac{1}{M} \sum_{m=1}^M \Delta_S^{(m)}$. As above, percentiles of the M samples provide credible interval for Δ_S .

In order to estimate Δ_P , an additional integration over the predictors is required. Wang et al. (2015) discuss the necessity of such an integration step when estimating population average causal effects with models that permit non-linearity and/or heterogeneity, and they propose the application of the Bayesian bootstrap to execute it. We adopt the same approach here. For each sample of the individual causal effects, $\{\Delta_O^{(m)}, \Delta_{O\perp}^{(m)}\}$, the Bayesian bootstrap is performed on it B times (where B is a large constant) and the average of each bootstrap sample taken to obtain B samples from the posterior distribution of the population average causal effect. Then, we randomly select a single one of these samples and call it $\Delta_P^{(m)}$, so that in the end we have collected $\{\Delta_P^{(1)}, \dots, \Delta_P^{(M)}\}$. The population average causal effect can then be estimated as $\hat{\Delta}_P = \frac{1}{M} \sum_{m=1}^M \Delta_P^{(m)}$ and the credible interval formed with the percentiles.

2.4 BART+SPL with Binary Outcomes

By invoking BART probit (Chipman et al., 2010) in the imputation stage and utilizing a simple arcsine transformation in the smoothing stage, we can straightforwardly extend BART+SPL to the binary outcomes setting. While most of our notation will remain the same for binary outcomes, we note that we now define the individual causal effects as $\Delta_i = P(Y_i(1) = 1) - P(Y_i(0) = 1)$ and the estimands as $\Delta_S = P(Y(1) = 1|\mathbf{X}) - P(Y(0) = 1|\mathbf{X})$ and $\Delta_P = E_{\mathbf{X}}[P(Y(1) = 1|\mathbf{X}) - P(Y(0) = 1|\mathbf{X})]$. Now we will fit a BART probit to estimate individual causal effects in O , fit a spline model to the arcsine transform of these estimates (which are bounded between -1 and 1), and use the spline to estimate individual causal effects for units in O^\perp . While we provide below explicit forms for the imputation and smoothing models in the binary setting, we refer the reader back to the previous section for the full sampling procedure details, which follow analogously to the continuous outcomes setting.

In the imputation stage, the BART probit model fit to the RO data has the following form:

$$P(Y_{Oq}^{obs} = 1) = \Phi\left(\sum_{j=1}^J g(E_{Oq}, \hat{\xi}_{Oq}, \mathbf{X}_{Oq}; \mathcal{T}_j, \mathcal{M}_j)\right),$$

where $\Phi()$ is the standard Normal cumulative distribution function. With this model, posterior samples $\tilde{P}(Y_{Oq}^{obs} = 1)$ and $\tilde{P}(Y_{Oq}^{mis} = 1)$ can be drawn and used to form a posterior sample of the individual causal effect, $\tilde{\Delta}_{Oq}$.

For the smoothing stage, as above, assume without loss of generality that all the units in O^\perp come from exposure group $e = 1$. Define $Y_{Oq}^*(1) = Y_{Oq}^{obs}$ if $E_{Oq} = 1$ and $Y_{Oq}^*(1) = I(\tilde{P}(Y_{Oq}^{mis} = 1) > 0.5)$ otherwise. Then the smoothing model is as follows:

$$\text{arcsine}(\tilde{\Delta}_{Oq}) = \mathbf{W}'\boldsymbol{\beta} + \epsilon_{Oq}, \quad \mathbf{W} = \begin{bmatrix} rcs(\hat{\xi}_{Oq}) \\ Y_{Oq}^*(1) \\ \mathbf{X}_{Oq} \end{bmatrix},$$

where $\epsilon_{Oq} \sim N(0, \sigma_S^2)$. Note that, unlike in the continuous case, no tuning parameter is included in the variance, as simulations indicated it was not needed to obtain reasonable coverage in the

binary setting. Individual causal effects on the arcsine scale for units in O^\perp can be obtained from the posterior predictive distribution and back-transformed to the desired scale. As described in the previous section, a second analogous smoothing model can be fit if O^\perp contains units from both the exposed and unexposed groups. Average causal effect estimation and uncertainty quantification proceed identically to the continuous case.

3 Simulations

3.1 Performance of BART+SPL with Continuous Outcomes

R code (R Core Team, 2016) to implement BART+SPL and to reproduce all simulations is available on Github at <https://github.com/rachelnethery/overlap>.

We purposely simulate data under a very challenging situation of: a) propensity score non-overlap; b) non-linearity of the potential outcomes in the propensity score; and c) and heterogeneous causal effects. We let $N = 500$ and assign exactly half of the subjects to $E = 1$. We generate two confounders that are highly associated with the exposure (E), one binary ($X_1 : X_1|E = 1 \sim \text{Bernoulli}(.5), X_1|E = 0 \sim \text{Bernoulli}(.4)$) and one continuous ($X_2 : X_2|E = 1 \sim N(1.25, 1), X_2|E = 0 \sim \text{Unif}(-c, c)$). The potential outcomes are then constructed as $Y_i(1) = (1 + \exp(-8X_{2i}) + 1)^{-1} + 0.25X_{1i}$ and $Y_i(0) = .85X_{2i} + 0.05X_{2i}^2 + 2$.

As is common in the literature, we use a simple logistic regression exposure model of the form $\text{logit}(P(E_i = 1)) = \beta_0 + \beta_1X_{1i} + \beta_2X_{2i}$ to estimate the propensity scores for all subjects. For each of the methods tested here, we utilize this same set of estimated propensity scores. This model is clearly misspecified, because, for example, the true relationship between E and X_2 is not linear. Thus, these simulations will provide insight into the relative performance of BART+SPL under mild propensity score model misspecification. In practice, when the form of the propensity score model is unknown, we encourage the use of flexible models for estimation (Westreich et al., 2010), such as BART, neural networks, boosting, or support vector machines, in order to reduce the chance of propensity score model misspecification. The use of BART for propensity score estimation is demonstrated in the application to real data in Section 4. Various flexible propensity score estimation methods could be tested and the method that achieves the best covariate balance selected.

The above data generating mechanisms simulate data sets with lack of overlap in the right tail of the propensity score (i.e., individuals from the unexposed group are unobserved or very sparse), and with varying degrees of non-overlap and non-linearity in the non-overlap region controlled by our choice of c . Our simulations are designed to produce non-overlap in the right tail of the propensity score distribution and our motivation is to demonstrate how our method performs in the presence of different features in this RN. Thus, simulated datasets are utilized in the results below only if any intervals of non-overlap outside the right tail contain 10 observations or fewer (cumulatively), and, in these datasets, the intervals of non-overlap outside the right tail are ignored (i.e., treated as part of the RO). In this way, we ensure that the results solely reflect how the tested methods respond to the features of the intended RN.

We consider three separate simulated scenarios, which are illustrated in Figure 3 in Section A.2 of the Appendix. In the first, referred to as 3.1A, the RN is quite small, and the trend in the individual causal effects in the RN is mildly non-linear (Figure 3a). In the second, referred to as 3.1B, the RN is somewhat larger and the trends exhibited by the individual causal effects in the RN are moderately non-linear (Figure 3b). In the final and most challenging scenario, called 3.1C, a substantial portion of the sample lies in the RN and the causal effects in the RN are highly non-linear (Figure 3c). These three settings are obtained by assigning $c = 1.85$, $c = 1.5$, and

$c = 1.15$, respectively. We use the interval-wise definition of overlap to define the RO and RN for each simulated dataset. The a and b parameters are specified as follows: $a = .1, b = 5$ in simulation 3.1A, $a = .15, b = 5$ in simulation 3.1B, and $a = .2, b = 5$ in simulation 3.1C.

We implement BART+SPL on 1,000 simulated datasets under each of the three conditions. Gutman and Rubin (2015) recommended a spline-based multiple imputation approach for estimating average causal effects. They also suggest trimming in conjunction with their method for samples suffering from non-overlap. We compared the performance of BART+SPL versus Gutman and Rubin’s method both with and without trimming (T-GR and U-GR, respectively) and also BART with and without trimming (T-BART and U-BART, respectively). Detailed results of the untrimmed analyses appear in Table 1 and the distributions of the average causal effect estimates from the trimmed and untrimmed analyses can be compared in Figure 4 in Section A.2 of the Appendix.

The simulation results demonstrate the dominant performance of BART+SPL compared to U-BART and U-GR under a wide range of challenging conditions, all involving mild propensity score model misspecification. However, simulation 3.1C reveals that, in extreme scenarios with dramatically non-linear trends in the RN, even the performance of BART+SPL deteriorates. Nonetheless, BART+SPL’s performance still far exceeds that of its competitors. In all three simulation scenarios, the trimmed estimates, which are no longer estimators of the population level causal effects, are most distant from the population level average causal effects and could easily lead to misinformed policy decisions.

Table 1: Absolute (Abs) bias, 95% credible interval coverage and mean square error (MSE) in estimation of the population average causal effects using each of the untrimmed methods applied to 1,000 simulated datasets with continuous outcome.

Simulation Setting	Method	Abs Bias	Abs Bias (%)	Coverage	MSE
3.1A	U-GR	0.10	5.28	0.00	0.05
	U-BART	0.09	4.60	0.02	0.11
	BART+SPL	0.03	1.46	1.00	0.02
3.1B	U-GR	0.12	6.49	0.00	0.07
	U-BART	0.15	7.96	0.00	0.19
	BART+SPL	0.05	2.56	0.99	0.02
3.1C	U-GR	0.15	8.20	0.00	0.08
	U-BART	0.23	12.32	0.00	0.32
	BART+SPL	0.09	4.74	0.66	0.06

The results in Table 1 also reveal the strengths and weaknesses of BART and splines when used separately. When extrapolation is easy (i.e., causal effects are only mildly non-linear in O^\perp) and the RN is small, BART performs comparably to the Gutman and Rubin spline method. However, as extrapolation becomes more difficult (i.e., more non-linear causal effects in O^\perp), the Gutman and Rubin splines are better able to extrapolate trends from the overlap region into the non-overlap region, and they, therefore, exhibit superior performance. By taking advantage of both the strong performance of BART in O and the spline’s ability to extrapolate in O^\perp , BART+SPL yields improved average causal effect estimates in the presence of propensity score non-overlap and heterogeneous causal effects.

3.2 Performance of BART+SPL with Binary Outcomes

In these simulations, $N = 1,000$ and E , X_1 , X_2 , and $\hat{\xi}$ are constructed as in Section 3.1. We let $\text{logit}(P(Y_i(1) = 1)) = (1 + \exp(-(8X_{2i} + 1)))^{-1} + 0.25X_{1i} - 2$ and $\text{logit}(P(Y_i(0) = 1)) = .85(X_{2i} - 1) + (X_{2i} - 1)^2$, and, to obtain binary outcomes, we simulate $Y_i(1) \sim \text{Bernoulli}(P(Y_i(1) = 1))$ and $Y_i(0) \sim \text{Bernoulli}(P(Y_i(0) = 1))$. As in the previous section, the resulting simulated datasets exhibit non-overlap in the right tail of the propensity score, and we can control the severity of the non-overlap as well as the severity of the non-linearity of the causal effects in the non-overlap region through the c parameter in the distribution of X_2 . Again, we will ignore any small intervals of non-overlap (containing less than 10 observations) that may occur due to randomness outside the right tail of the propensity score. We consider the following 3 simulated scenarios, which have properties similar to those of the three simulations described in the previous section: simulation 3.2A with $c = 1.85$, simulation 3.2B with $c = 1.5$, and simulation 3.2C with $c = 1.15$. A sample dataset under each of these conditions is illustrated in Figure 5 in Section A.2 of the Appendix.

We implement BART+SPL, U-GR, and U-BART on each of 1,000 simulated datasets under each condition. The results appear in Table 2. Although all of the methods demonstrate larger percent bias in these simulations compared to the continuous outcome simulations, we still see consistent and substantial improvements in bias, coverage, and MSE of the population average causal effects with BART+SPL over U-GR and U-BART.

Table 2: Absolute (Abs) bias, 95% credible interval coverage, and mean square error (MSE) in estimation of the population average causal effects using each of the untrimmed methods applied to 1,000 simulated datasets with binary outcome.

Simulation Setting	Method	Abs Bias	Abs Bias (%)	Coverage	MSE
3.2A	U-GR	0.07	15.72	0.14	0.05
	U-BART	0.08	17.49	0.41	0.04
	BART+SPL	0.05	11.83	0.73	0.02
3.2B	U-GR	0.11	25.95	0.02	0.07
	U-BART	0.09	21.32	0.31	0.04
	BART+SPL	0.06	14.61	0.70	0.02
3.2C	U-GR	0.15	36.87	0.01	0.10
	U-BART	0.10	24.91	0.29	0.04
	BART+SPL	0.09	21.03	0.69	0.03

3.3 BART+SPL with High Dimensional Covariates

One of the most widely-recognized limitations of BART, which was noted by its developers (Chipman et al., 2010), is its poor performance (under default model specifications) when the number of predictors, p , is large. The decline in performance is most significant when many irrelevant predictors (i.e., predictors unrelated to the outcome) are included. Thus, in this section, we seek to examine whether and how BART+SPL should be applied in settings where the number of potential confounders is large. Although BART has been extended to permit sparsity in the $p > N$ setting (Linerio, 2016), we do not consider the $p > N$ case here.

For these simulations, we let $N = 1,000$ and assign exactly half of the sample to $E = 1$. We then generate 10 confounders, 5 binary and 5 continuous. The binary confounders have distribution $X_1|E = 1, \dots, X_5|E = 1 \sim \text{Bernoulli}(.45)$, $X_1|E = 0, \dots, X_5|E = 0 \sim \text{Bernoulli}(.4)$, and the continuous confounders have distribution $X_6|E = 1, \dots, X_{10}|E = 1 \sim N(1.25, 9)$, $X_6|E = 0, \dots, X_{10}|E =$

$0 \sim Unif(-2, 2.5)$. We consider the following three scenarios: only these 10 confounders are present (simulation 3.3A), these 10 confounders as well as 10 randomly generated “potential confounders” are present (simulation 3.3B), and these 10 confounders as well as 20 randomly generated “potential confounders” are present (simulation 3.3C). Of course, in real applications, we often do not know a priori which of the potential confounders are true confounders, hence we include them all in the modeling. A propensity score is formed using predicted probabilities from the logistic regression $\text{logit}(P(E_i = 1)) = \mathbf{Z}_i\boldsymbol{\beta}$, where \mathbf{Z}_i is a vector of the true and potential confounders (if any are used). The potential outcomes are generated so that they exhibit non-linear trends in the estimated propensity score— $Y_i(0) = 5 + .2X_{1i} + .2X_{2i} + .2X_{3i} + .2X_{4i} + .2X_{5i} + (1 + \exp(-8X_{6i} + 1))^{-1} + X_{7i} + X_{8i} + X_{9i} + X_{10i}$ and $Y_i(1) = -5 + .2X_{1i} + .2X_{2i} + .2X_{3i} + .2X_{4i} + .2X_{5i} - .5X_{6i} - .5X_{7i} - .5X_{8i} - .5X_{9i} - .5X_{10i}$.

The features of these data are illustrated in Figure 6 in Section A.2 of the Appendix. The simulations are designed to have a large RN in the right tail of the propensity score, with moderate non-linearity in the causal effect in the RN. In each simulated dataset, we define the RO and RN using the interval-wise overlap definition with $a = .15, b = 5$.

We simulate 1,000 datasets from each of the three scenarios described above. We first execute BART+SPL as we did in the previous section— including the propensity score and all potential confounders as predictors. We also implement a modification of BART+SPL which uses the propensity score as a predictor but includes none of the potential confounders (PBART+SPL). Finally, we apply the untrimmed Gutman and Rubin spline method (GR) for comparison. Results are provided in Table 3.

Table 3: Absolute (Abs) bias, 95% credible interval coverage, and mean square error (MSE) in estimation of the population average causal effects using BART+SPL, PBART+SPL, and GR applied to simulations 3.2A, 3.2B, and 3.2C

Simulation Setting	Method	Abs Bias	Abs Bias (%)	Coverage	MSE
3.3A	GR	0.48	3.08	0.01	5.93
	BART+SPL	0.32	2.07	0.81	2.90
	PBART+SPL	0.82	5.27	0.04	9.21
3.3B	GR	0.59	3.79	0.00	6.76
	BART+SPL	1.23	7.93	0.01	11.23
	PBART+SPL	0.91	5.91	0.01	10.23
3.3C	GR	0.69	4.43	0.00	7.77
	BART+SPL	1.64	10.57	0.00	17.86
	PBART+SPL	1.01	6.52	0.00	11.45

These results reflect BART’s struggle in the presence of irrelevant predictors. When only the 10 true confounders are included in the modeling, BART+SPL outperforms GR and PBART+SPL and demonstrates similar performance as in Section 3.1. However, when either 10 or 20 irrelevant predictors are introduced, BART+SPL gives the poorest results of the three methods. While PBART+SPL provides some improvement over BART+SPL in these settings, it falls short of GR, whose performance declines very little as more irrelevant predictors are added. These results should serve as a warning that BART+SPL is only likely to improve on existing methods in settings where the set of true confounders can be posited a priori with some confidence.

3.4 Guidelines for Defining the RN

The simulation results in this section are intended to provide guidance on both the degree of non-overlap that threatens BART’s performance and the degree of non-overlap that threatens

BART+SPL’s performance. While not intended to be conclusive, these insights may be able to be applied in real data settings to inform the choice of method used and the definition the RO and RN (i.e., the choice of a and b in the non-overlap definition) that is most appropriate.

To impose strict control on the size of the RO and RN, in these simulations we utilize a single confounder rather than a propensity score. Based on the above simulations, we expect the performance of BART (and BART+SPL) in settings with small and moderate numbers of confounders to be similar, as long as all the covariates considered are true confounders. Thus, the insights gained from these single confounder simulations are likely to scale well to scenarios with moderate numbers of confounders.

We let $N = 500$ and assign half of the sample to $E = 1$. We generate the confounder as $X|E = 1 \sim N(2.5, 4)$, $X|E = 0 \sim N(v, w)$, where v and w control the degree of non-overlap. Unlike in the previous simulations, in these we generate a single, fixed instance of the confounder and simply add random noise to (a function of) it to create the potential outcomes for each simulation. We consider two potential outcome scenarios, one of which produces data that are relatively simple to model (with BART) while the other produces data that are challenging to model. The former, which we label simulation 3.4A, is created by assigning $Y(0) = 1.5 + \frac{X+(X^2/2!)}{20} + N(0, 0.06)$ and $Y(1) = \frac{1}{1+e^{-(X-1)}} + N(0, 0.06)$ and the latter, which we call simulation 3.4B, by $Y(0) = 1.5 + \frac{X+(X^2/2!)+(X^3/3!)}{20} + N(0, 0.06)$ and $Y(1) = \frac{1}{1+e^{-(X-1)}} + N(0, 0.06)$.

In both simulation 3.4A and 3.4B, we achieve different degrees of non-overlap, primarily non-overlap in the right tail of the confounder, by manipulating v and w . In order from least to most non-overlap, we consider $\{v = 1.4, w = 1.96\}$, $\{v = 0.75, w = 1.44\}$, and $\{v = 0, w = 1\}$. Moreover, in each scenario, we test the following three specifications of $\{a, b\}$ in the definition of the RO, in order from most to least conservative: $\{a = 0.05 * (range(X)), b = 10\}$, $\{a = 0.1 * (range(X)), b = 10\}$, and $\{a = 0.15 * (range(X)), b = 3\}$. Considering each combination of $\{v, w\}$ and $\{a, b\}$ leads to 9 different settings for each of simulation 3.4A and 3.4B, for a total of 18 simulations. The proportion of the sample falling into the RN, denoted π in these simulations ranges from $\pi = 6\%$ to $\pi = 39\%$. Of course, the impact of non-overlap on average causal effect estimates depends not only on the proportion of the sample falling in the RN but also likely on the extremity of the observations in the RN relative to the RO. In our simulations, as π increases, the average distance between observations in the RO and the RN also increases. An example dataset from both simulation 3.4A and simulation 3.4B is presented in Figure 7 in Section A.2 of the Appendix.

We apply BART+SPL to 1,000 simulated datasets under each of the 18 conditions, and we apply BART alone (ignoring the non-overlap) for each specification of $\{v, w\}$. Table 4 and Table 5 contain the results for simulations 3.4A and 3.4B, respectively. We first remark that, while BART+SPL nearly always performs better in terms of each metric than BART, the most notable difference in the BART+SPL and BART results is the difference in coverage probabilities, with BART+SPL consistently obtaining conservative coverage and BART’s coverage deteriorating as the degree of non-overlap increases. Even when only 6% of the data falls into the RN, BART’s coverage is unreliable. Thus, BART could provide misleading inference even with small amounts of non-overlap.

BART+SPL’s coverage is reliable in all the simulations assessed, however its bias tends to increase as the degree of non-overlap increases. Thus, it appears that, if some bias in the point estimate can be tolerated, BART+SPL can be expected to provide conservative inference in (non-pathological) scenarios with over 25% of the data in the RO. However, based on the observation that BART+SPL’s bias is greater than 5% in simulation 3.4B under each RO definition with $\{v = 0.75, w = 1.44\}$ and $\{v = 0, w = 1\}$, a more conservative option might be to sacrifice the population-level estimand and performed a trimmed or weighted analysis when more than 15%

Table 4: Absolute (Abs) bias, 95% credible interval coverage, and mean square error (MSE) in estimation of the population average causal effects using BART+SPL and BART applied to simulation 3.4A. RO-1 refers to simulations with the RO defined as $a = 0.05 * (\text{range}(X))$, $b = 10$, RO-2 refers to simulations with the RO defined as $a = 0.1 * (\text{range}(X))$, $b = 10$, and RO-3 refers to simulations with the RO defined as $a = 0.15 * (\text{range}(X))$, $b = 3$.

v, w	Method	π	Abs Bias	Abs Bias (%)	Coverage	MSE
$v = 1.4, w = 1.96$	BART+SPL, RO-1	17	0.03	2.27	1.00	0.07
	BART+SPL, RO-2	11	0.02	2.11	1.00	0.07
	BART+SPL, RO-3	6	0.02	1.99	1.00	0.07
	BART		0.03	2.93	0.83	0.09
$v = 0.75, w = 1.44$	BART+SPL, RO-1	25	0.04	3.72	1.00	0.09
	BART+SPL, RO-2	15	0.04	3.27	1.00	0.08
	BART+SPL, RO-3	13	0.04	3.31	1.00	0.08
	BART		0.06	5.44	0.48	0.11
$v = 0, w = 1$	BART+SPL, RO-1	39	0.07	5.71	1.00	0.10
	BART+SPL, RO-2	21	0.05	4.62	1.00	0.09
	BART+SPL, RO-3	19	0.05	4.64	1.00	0.09
	BART		0.07	6.30	0.57	0.11

of the data falls in the RN.

Finally, we note that the results, particularly for simulation 3.4B, indicate that one should avoid defining the RO too conservatively, as the discarding of too much information can lead to increased bias. The moderate choice of $a = 0.1 * \text{range}(X)$ and $b = 10$ provides the best results in most of the simulations.

4 The Effect of Natural Gas Compressor Stations on County-Level Thyroid Cancer and Leukemia Mortality

During the last several decades, the United States has witnessed a sharp increase in the incidence of thyroid cancer, with thyroid cancer now accounting for 1-1.5% of all newly diagnosed cancer cases (Pellegriti et al., 2013). Increased exposure of the population to radiation and carcinogenic environmental pollutants is blamed, in part, for this increase.

During the last several decades, US natural gas (NG) production has also increased rapidly. NG production and distribution systems have recently received attention as a potential source of human exposure to carcinogenic environmental pollutants, such as benzene. Benzene is known to cause leukemia (Smith, 1996), and recent epidemiological studies have, indeed, found links between natural gas production and leukemia (Finkel, 2016; McKenzie et al., 2017b). NG production is also known to release numerous endocrine-disrupting chemicals (Kassotis et al., 2016). A recent study compared thyroid cancer incidence in Pennsylvania counties before and after the initiation of unconventional NG drilling (also known as fracking) in the area and found significant increases in incidence (Finkel, 2016). This relationship between NG systems and thyroid cancer could be of particular interest due to the coincident increase in US thyroid cancer incidence and US NG production.

Most previous studies of the health effects of NG systems have focused on associations between residential proximity to production sites (i.e., drilling wells) and health outcomes (Finkel, 2016; Rasmussen et al., 2016; McKenzie et al., 2017b). In this study, we turn our attention instead to the

Table 5: Absolute (Abs) bias, 95% credible interval coverage, and mean square error (MSE) in estimation of the population average causal effects using BART+SPL and BART applied to simulation 3.4B. RO-1 refers to simulations with the RO defined as $a = 0.05 * (\text{range}(X))$, $b = 10$, RO-2 refers to simulations with the RO defined as $a = 0.1 * (\text{range}(X))$, $b = 10$, and RO-3 refers to simulations with the RO defined as $a = 0.15 * (\text{range}(X))$, $b = 3$.

v, w	Method	π	Abs Bias	Abs Bias (%)	Coverage	MSE
$v = 1.4, w = 1.96$	BART+SPL, RO-1	17	0.05	4.53	1.00	0.11
	BART+SPL, RO-2	11	0.04	4.23	1.00	0.11
	BART+SPL, RO-3	6	0.04	3.72	1.00	0.10
	BART		0.05	4.69	0.60	0.12
$v = 0.75, w = 1.44$	BART+SPL, RO-1	25	0.07	6.19	1.00	0.14
	BART+SPL, RO-2	15	0.06	5.50	1.00	0.13
	BART+SPL, RO-3	13	0.06	5.74	1.00	0.13
	BART		0.07	6.72	0.34	0.14
$v = 0, w = 1$	BART+SPL, RO-1	39	0.08	7.42	1.00	0.14
	BART+SPL, RO-2	21	0.06	5.78	1.00	0.12
	BART+SPL, RO-3	19	0.06	5.72	1.00	0.12
	BART		0.06	5.76	0.73	0.12

question of the health effects of NG distribution systems. Specifically, we aim to provide the first data-driven epidemiological investigation of the effects of proximity to NG compressor stations on thyroid cancer and leukemia mortality rates.

NG compressor stations are pumping stations located at 40-70 mile intervals along NG pipelines. They keep pressure in the pipelines so that NG continues flowing in the desired direction (Messersmith et al., 2015). Aspects of the operations at the compressor stations have raised health and safety concerns both for workers and for residents of nearby communities (Southwest Pennsylvania Environmental Health Project, 2015). In this paper, we will exclude from consideration the health and safety concerns related to accidents at compressor stations (of which many have been documented) and focus on the potentially harmful exposures to nearby communities resulting from the normal operations of compressor stations. Fugitive emissions, or unintended leaking of chemicals from the compressor station equipment, are known to occur but are not well-characterized. NG compressor stations also routinely conduct “blowdowns”, in which pipelines and equipment are vented to reduce pressure (Kloczko, 2015). Any chemicals present in the pipeline during a blowdown are reportedly released into the air in a 30-60 meter plume of gas (Southwest Pennsylvania Environmental Health Project, 2015). Again, poor documentation of this process has resulted in difficulty characterizing the specific types of chemicals emitted.

While airborne emissions from compressor stations are regulated by the EPA under the Clean Air Act (Messersmith et al., 2015), air quality studies in Pennsylvania and Texas have discovered harmful chemicals in excess of standards near NG compressor stations (Wolf Eagle Environmental, 2009; Pennsylvania Department of Environmental Protection, 2010). These chemicals include methane, ethane, propane, butane, m and p xylene, and numerous benzene compounds. Benzene is a known carcinogen (Maltoni et al., 1989; Golding and Watson, 1999) and many of these compounds are known or suspected endocrine disruptors (EPA, 2018). Motivated by these concerning findings, we present an investigation of the effects of compressor stations on county-level thyroid cancer and leukemia mortality rates.

We collected 2014 thyroid cancer and leukemia mortality rate estimates for each county in

the US from the Global Health Data Exchange. The data and methods used to develop these estimates have been described previously (Mokdad et al., 2017). We also obtained the locations of NG compressor stations from publicly available data compiled by Oak Ridge National Laboratory (Oak Ridge National Laboratory, 2017). While the data is not guaranteed to be complete, it is, to our knowledge, the most comprehensive documentation of compressor station locations in existence, with 1,359 compressor station locations verified using imagery. In order to test a causal hypothesis, we need to assume that exposure to compressor station-related emissions preceded 2014 (the year for which cancer mortality rates are observed) by at least the minimum latency period for thyroid cancer and leukemia. The CDC reports the minimum latency period for thyroid cancer as 2.5 years and the minimum latency for leukemia as 0.4 years (World Trade Center Health Program, 2015). Although the dataset does not contain dates of origin for the compressor stations, it does contain peak operation dates, and we know the stations must have been operational by that date (and likely before that date). 84% of the compressor stations in the dataset have peak operating dates in or before 2012; thus, it seems reasonable to assume that most of the compressor stations in the dataset operated at least 2.5 years prior to 2014.

Our county-level exposure variable is an indicator of whether a compressor station is present in the county. We collected county-level demographic, socio-economic, and behavioral confounder data from the American Community Survey 2014 5-year estimates (US Census Bureau, 2014) and the 2014 County Health Rankings and Roadmaps (Robert Wood Johnson Foundation, 2014). Data were accessed using Social Explorer. The confounders used are rate of primary care physicians, percent of less than 65 year olds uninsured, percent diabetic, percent current smokers, percent of people with limited access to healthy foods, percent obese, food environment index, population density, percent male, percent less than age 55, percent white, average household size, percent with bachelor’s degree or higher, percent unemployed, median household income, Gini index of inequality, percent owner-occupied housing units, median rent as proportion of income, and average commute time to work. All the data used in this analysis are publicly available, and the data and R code to reproduce the analysis are posted on Github at <https://github.com/rachelnethery/overlap>.

We note that the sensitivity of this analysis to detect exposure effects will be low, because any true health effects of exposure to compression station emissions is likely more spatially concentrated than the county level. Although a higher spatial resolution analysis would be preferable, obtaining important behavioral confounder data at a finer spatial resolution across large geographic regions is challenging. In an effort to improve the detectability of effects, we focus our analysis on roughly the mid-western region of the US (counties with centroid longitudes between -110 and 90), where few other sources of pollution exist compared to the coastal regions (Di et al., 2017). A focus on this region is also reasonable because NG production has a much longer history in this region compared to the other large NG production hub in the US, the Marcellus Shale in Pennsylvania and West Virginia, which only began to be developed in the late 2000s. Thus, the infrastructure is likely to have been in place for longer, leading to greater exposure of populations in this region.

We begin with a dataset of 1,309 counties, and, after discarding counties with any missing confounders, are left with $N=978$ counties. 291 of these counties are exposed (i.e., contain at least one natural gas compressor) while 687 are unexposed. Table 7 in Section A.2 of the Appendix shows the differences in the exposed and unexposed populations. Notably, exposed counties have higher percent uninsured, lower population density, lower percent white, lower education, and higher percent unemployment. We estimate a propensity score by applying a BART probit with exposure status as the response and all the confounders as predictors. The histogram in Figure 1 illustrates the non-overlap in the resulting propensity score, with the solid vertical lines denoting the start of the intervals of non-overlap that are detected in each tail of the propensity score using the interval-wise overlap definition and $a = 0.1 * range(\hat{\xi})$ and $b = 10$. With these specifications,

13% of the sample falls into the RN. BART+SPL is needed to obtain population level causal effect estimates in this setting.

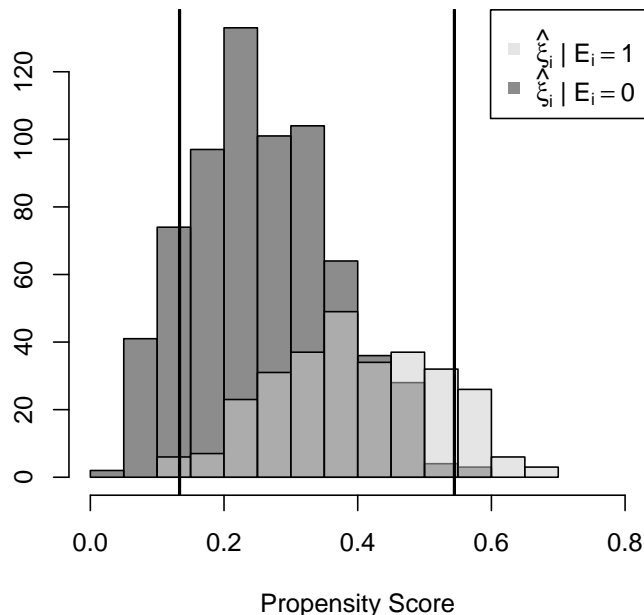


Figure 1: Propensity score histograms stratified by exposure status and overlaid. Bold vertical lines represent the start of non-overlap intervals in both tails of the distribution.

The following outcomes variables are considered: (1) 2014 thyroid cancer mortality rate, (2) the change in thyroid cancer mortality rate from 1980 to 2014, (3) 2014 leukemia mortality rate, and (4) the change in leukemia mortality rate from 1980 to 2014. The 2014 rates are log-transformed prior to analysis. We analyze each outcome using both BART+SPL and trimmed BART. Investigation of the features of the trimmed sample reveals, most notably, that the counties in the trimmed sample are more urban and densely populated, on average, than the population represented by the full sample (trimmed sample population density is 110.44 compared to 99.38 in the full sample).

Average causal effect estimates and 95% credible intervals from each analysis can be found in Table 6. The BART+SPL analysis is estimating population average causal effects, and the trimmed BART is estimating trimmed sample average causal effects. Only one of these analyses finds statistically significant effects of NG compressor stations– the trimmed BART analysis of the change in thyroid cancer mortality rates from 1980 to 2014. As discussed above, we must interpret this as a significant effect only in the trimmed sample, which is on average more urban than the population of interest. The population-level estimates from BART+SPL have wider credible intervals for two reasons. First, the additional marginalization over the confounders required to obtain population-level estimates increases the variance. Second, to estimate at the population level, we must account for the additional uncertainty induced by the non-overlap, which BART+SPL does by inflating variances in the RN. With these wide credible intervals, evidence of an effect must be very compelling in order to achieve statistical significance. However, we note that the point estimate from each analysis is positive, indicating a harmful average effect of compressor stations on health,

and in each case the point estimates are quite similar in the trimmed and untrimmed analyses.

Table 6: Average causal effects of natural gas compressor station presence on 2014 county-level thyroid cancer and leukemia mortality rates and the change in thyroid cancer and leukemia mortality rates from 1980 to 2014.

Outcome	Method	Effect	95% CI
2014 Thyroid Rates	BART+SPL	0.002	-0.017, 0.020
	BART	0.002	-0.007, 0.011
Change in Thyroid Rates 1980-2014	BART+SPL	1.034	-0.176, 2.271
	BART	1.071	0.128, 2.025
2014 Leukemia Rates	BART+SPL	0.003	-0.015, 0.021
	BART	0.005	-0.004, 0.014
Change in Leukemia Rates 1980-2014	BART+SPL	0.900	-0.374, 2.132
	BART	0.957	-0.007, 1.917

The significant finding in the trimmed sample suggests that the health effects of compressor station exposure is a topic that warrants further study with higher quality data. The data utilized here have numerous limitations that could be improved upon by future studies. In particular, an analysis at higher spatial resolution is needed in order to be able to detect geographically concentrated effects that may be washed out at the county level. Moreover, counties with compressor stations may also be more likely to be located in NG production regions; thus, an analysis at the county level may not be able to distinguish the effects of compressor station exposure from the effects of NG drilling and production-related exposures. Finally, an investigation of cancer diagnosis rates may be more informative about the possible dangers of NG compressor station exposure than our investigation of cancer mortality rates. However, cancer diagnosis rates are difficult to obtain across large geographic regions.

5 Discussion

In this paper, we have introduced a general definition of propensity score non-overlap and have proposed a Bayesian modeling approach to estimate population average causal effects and corresponding uncertainties in the presence of propensity score non-overlap and heterogeneous causal effects. A novel feature of our proposed approach is its separation of the tasks of estimating causal effects in the region of overlap and the region of non-overlap and its delegation of these tasks to two distinct models. A BART model is selected to perform estimation of individual causal effects in the region of overlap where there is strong data support, thanks to its non-parametric nature, which is consistent with classic causal inference approaches, its lack of dependence on user model specification, its ability to capture non-linear and heterogeneous effects, and its demonstrated strong predictive capacity. In the region of non-overlap, where reliance on model specification is required to identify causal effects, individual causal effects are estimated by extrapolating trends from the region of overlap via a parametric spline model. This approach, which we call BART+SPL, can be applied to data with either continuous or binary outcomes and can be implemented in a fully Bayesian manner, so that uncertainties from both stages are captured.

We demonstrated via simulations that BART+SPL outperforms both stand-alone BART and stand-alone spline causal inference approaches in estimation of population average causal effects under a wide range of conditions involving propensity score non-overlap. However, due to BART's

limitations in high dimensional settings, BART+SPL may give more biased results than existing methods when many irrelevant predictors are present.

A key contribution of our work is the introduction of a tuning parameter used to inflate the variance of causal effect estimates in regions of poor data support, so that this variance adequately reflects the high estimation uncertainty in such regions. We have recommended a choice of tuning parameter that linearly increases the variance as the distance into the RN increases, and the scale of these increases is tailored to correspond reasonably to the scale of the estimated causal effects in regions of good data support. Simulation results demonstrated that the resulting credible intervals are much more reliable than those produced by competing methods in the presence of non-overlap. However, in “simple” scenarios (i.e., scenarios where trends in the causal effects in the RN are easily predictable based on trends in the RO), this tuning parameter can produce conservative uncertainties.

Our work introduces an exciting direction for methodological developments in the context of causal inference with propensity score non-overlap. For instance, other machine learning methods (Cristianini and Shawe-Taylor, 2000; Breiman, 2001; Schmidhuber, 2015) may also have properties that make them well-suited to handle non-overlap, and the replacement of BART with one of these other methods could be explored. Moreover, the limitations of BART in high dimensions provide an opportunity for improvement on our method. Improvements might be made through the use of other machine learning methods, through the integration of sparsity-inducing priors with BART as developed by Linero (2016), or through the addition of pre-processing procedures to first identify a minimal confounder set. Finally, theoretical results remain to be developed for methods that perform causal effect estimation in the RO and RN using separate models. These could be avenues for future work.

6 Acknowledgements

Support for this work was provided by NIH grants P01CA134294, R01GM111339, R35CA197449, R01ES026217, P50MD010428, R01ES028033, and R01MD012769. The authors also received support from EPA grants 83615601 and 83587201-0, and Health Effects Institute grant 4953-RFA14-3/16-4.

References

- Austin, P. C. (2011, May). An Introduction to Propensity Score Methods for Reducing the Effects of Confounding in Observational Studies. *Multivariate Behavioral Research* 46(3), 399–424.
- Biau, G., L. Devroye, and G. Lugosi (2008). Consistency of random forests and other averaging classifiers. *Journal of Machine Learning Research* 9(Sep), 2015–2033.
- Bonato, V., V. Baladandayuthapani, B. M. Broom, E. P. Sulman, K. D. Aldape, and K.-A. Do (2011). Bayesian ensemble methods for survival prediction in gene expression data. *Bioinformatics* 27(3), 359–367.
- Breiman, L. (1996). Bagging predictors. *Machine Learning* 24(2), 123–140.
- Breiman, L. (2001). Random forests. *Machine learning* 45(1), 5–32.
- Bühlmann, P. and B. Yu (2002). Analyzing bagging. *Annals of Statistics* 30(4), 927–961.

- Chipman, H. A., E. I. George, and R. E. McCulloch (1998, September). Bayesian CART Model Search. *Journal of the American Statistical Association* 93(443), 935–948.
- Chipman, H. A., E. I. George, and R. E. McCulloch (2010, March). BART: Bayesian additive regression trees. *The Annals of Applied Statistics* 4(1), 266–298.
- Cochran, W. G. and D. B. Rubin (1973). Controlling bias in observational studies: A review. *Sankhyā: The Indian Journal of Statistics, Series A* 35(4), 417–446.
- Cole, S. R. and M. A. Hernn (2008, September). Constructing Inverse Probability Weights for Marginal Structural Models. *American Journal of Epidemiology* 168(6), 656–664.
- Cristianini, N. and J. Shawe-Taylor (2000). *An introduction to support vector machines and other kernel-based learning methods*. Cambridge university press.
- Crump, R. K., V. J. Hotz, G. W. Imbens, and O. A. Mitnik (2006). Moving the goalposts: Addressing limited overlap in the estimation of average treatment effects by changing the estimand. Working Paper 330, National Bureau of Economic Research.
- Crump, R. K., V. J. Hotz, G. W. Imbens, and O. A. Mitnik (2009, March). Dealing with limited overlap in estimation of average treatment effects. *Biometrika* 96(1), 187–199.
- D’Amour, A., P. Deng, A. Feller, L. Lei, and J. Sekhon (2017). Overlap in observational studies with high-dimensional covariates. *arXiv preprint arXiv:1711.02582*.
- Dehejia, R. H. and S. Wahba (1999). Causal effects in nonexperimental studies: Reevaluating the evaluation of training programs. *Journal of the American statistical Association* 94(448), 1053–1062.
- Di, Q., Y. Wang, A. Zanobetti, Y. Wang, P. Koutrakis, C. Choirat, F. Dominici, and J. D. Schwartz (2017). Air pollution and mortality in the medicare population. *New England Journal of Medicine* 376(26), 2513–2522.
- EPA, U. (2018). Endocrine disruptor screening program (edsp) estrogen receptor bioactivity. <https://www.epa.gov/endocrine-disruption/endocrine-disruptor-screening-program-edsp-estrogen-receptor-bioactivity#main-content>. Accessed: 2018-03-27.
- Ferguson, K. K., T. F. McElrath, and J. D. Meeker (2014). Environmental phthalate exposure and preterm birth. *JAMA pediatrics* 168(1), 61–68.
- Finkel, M. (2016). Shale gas development and cancer incidence in southwest pennsylvania. *Public health* 141, 198–206.
- Fisher, R. (1935). *Design of Experiments*. Oliver and Boyd.
- Friedman, J., T. Hastie, and R. Tibshirani (2000). Additive logistic regression: a statistical view of boosting (with discussion and a rejoinder by the authors). *The Annals of Statistics* 28(2), 337–407.
- Friedman, J. H. (2001). Greedy function approximation: a gradient boosting machine. *Annals of statistics* (5), 1189–1232.

- Golding, B. and W. Watson (1999). Possible mechanisms of carcinogenesis after exposure to benzene. *IARC scientific publications* (150), 75–88.
- Gutman, R. and D. B. Rubin (2015). Estimation of causal effects of binary treatments in unconfounded studies. *Statistics in Medicine* 34(26), 3381–3398.
- Hastie, T. and R. Tibshirani (2000). Bayesian backfitting. *Statistical Science* 15(3), 196–223.
- He, S., X. Li, M. R. Viant, and X. Yao (2009). Profiling ms proteomics data using smoothed non-linear energy operator and bayesian additive regression trees. *Proteomics* 9(17), 4176–4191.
- Hill, J. and Y.-S. Su (2013). Assessing lack of common support in causal inference using bayesian nonparametrics: Implications for evaluating the effect of breastfeeding on children’s cognitive outcomes. *The Annals of Applied Statistics*, 1386–1420.
- Hill, J. L. (2011, January). Bayesian Nonparametric Modeling for Causal Inference. *Journal of Computational and Graphical Statistics* 20(1), 217–240.
- Ho, D. E., K. Imai, G. King, and E. A. Stuart (2007). Matching as nonparametric preprocessing for reducing model dependence in parametric causal inference. *Political analysis* 15(3), 199–236.
- Huang, J., E. Marco, L. Pinello, and G.-C. Yuan (2015). Predicting chromatin organization using histone marks. *Genome Biology* 16(1), 162.
- Kassotis, C. D., D. E. Tillitt, C.-H. Lin, J. A. McElroy, and S. C. Nagel (2016). Endocrine-disrupting chemicals and oil and natural gas operations: potential environmental contamination and recommendations to assess complex environmental mixtures. *Environmental health perspectives* 124(3), 256.
- Kindo, B. P., H. Wang, and E. A. Peña (2016). Multinomial probit bayesian additive regression trees. *Stat* 5(1), 119–131.
- King, G. and L. Zeng (2005). The dangers of extreme counterfactuals. *Political Analysis* 14(2), 131–159.
- Kloczko, N. (2015). Summary on compressor stations and health impacts. <http://www.environmentalhealthproject.org/files/A%20Brief%20Review%20of%20Compressor%20Stations%2011.2015.pdf>. Accessed: 2018-03-27.
- LaLonde, R. J. (1986). Evaluating the econometric evaluations of training programs with experimental data. *The American Economic Review* 76(4), 604–620.
- Li, F., K. L. Morgan, and A. M. Zaslavsky (2017). Balancing Covariates via Propensity Score Weighting. *Journal of the American Statistical Association*, 1–11.
- Lin, Y. and Y. Jeon (2006). Random forests and adaptive nearest neighbors. *Journal of the American Statistical Association* 101(474), 578–590.
- Linero, A. R. (2016, December). Bayesian Regression Trees for High Dimensional Prediction and Variable Selection. *Journal of the American Statistical Association* 0.
- Liu, Y., Z. Shao, and G.-C. Yuan (2010). Prediction of polycomb target genes in mouse embryonic stem cells. *Genomics* 96(1), 17–26.

- Liu, Y., M. Traskin, S. A. Lorch, E. I. George, and D. Small (2015). Ensemble of trees approaches to risk adjustment for evaluating a hospitals performance. *Health care management science* 18(1), 58–66.
- Loh, W.-Y. (2014). Fifty years of classification and regression trees. *International Statistical Review* 82(3), 329–348.
- Lunt, M. (2014, January). Selecting an Appropriate Caliper Can Be Essential for Achieving Good Balance With Propensity Score Matching. *American Journal of Epidemiology* 179(2), 226–235.
- Maltoni, C., A. Ciliberti, G. Cotti, B. Conti, and F. Belpoggi (1989). Benzene, an experimental multipotential carcinogen: results of the long-term bioassays performed at the bologna institute of oncology. *Environmental health perspectives* 82, 109.
- McKenzie, L. M., W. B. Allshouse, T. E. Byers, E. J. Bedrick, B. Serdar, and J. L. Adgate (2017a). Childhood hematologic cancer and residential proximity to oil and gas development. *PLOS ONE* 12(2), e0170423.
- McKenzie, L. M., W. B. Allshouse, T. E. Byers, E. J. Bedrick, B. Serdar, and J. L. Adgate (2017b). Childhood hematologic cancer and residential proximity to oil and gas development. *PloS one* 12(2), e0170423.
- Messersmith, D., D. Brockett, and C. Loveland (2015). Understanding natural gas compressor stations. *Penn State Extension*.
- Mokdad, A. H., L. Dwyer-Lindgren, C. Fitzmaurice, R. W. Stubbs, A. Bertozzi-Villa, C. Morozoff, R. Charara, C. Allen, M. Naghavi, and C. J. Murray (2017). Trends and patterns of disparities in cancer mortality among us counties, 1980-2014. *Jama* 317(4), 388–406.
- Neyman, J. (1923). On the application of probability theory to agricultural experiments. essay on principles. section 9.(translated and edited by dm dabrowska and tp speed, statistical science (1990), 5, 465-480). *Annals of Agricultural Sciences* 10, 1–51.
- Oak Ridge National Laboratory (2017). Natural gas compressor stations. https://hifld-dhs-gii.opendata.arcgis.com/datasets/fd7d62905d194eba87d2ee18d1a244b3_0. Accessed: 2018-03-29.
- Pellegriti, G., F. Frasca, C. Regalbuto, S. Squatrito, and R. Vigneri (2013). Worldwide increasing incidence of thyroid cancer: update on epidemiology and risk factors. *Journal of Cancer Epidemiology* 2013.
- Pennsylvania Department of Environmental Protection (2010). Southwestern pennsylvania marcellus shale short-term ambient air sampling report. http://www.dep.state.pa.us/dep/deputate/airwaste/aq/aqm/docs/Marcellus_SW_11-01-10.pdf. Accessed: 2018-03-29.
- Petersen, M. L., K. E. Porter, S. Gruber, Y. Wang, and M. J. van der Laan (2012, February). Diagnosing and responding to violations in the positivity assumption. *Statistical Methods in Medical Research* 21(1), 31–54.
- R Core Team (2016). *R: A Language and Environment for Statistical Computing*. Vienna, Austria: R Foundation for Statistical Computing.

- Rasmussen, S. G., E. L. Ogburn, M. McCormack, J. A. Casey, K. Bandeen-Roche, D. G. Mercer, and B. S. Schwartz (2016). Association between unconventional natural gas development in the marcellus shale and asthma exacerbations. *JAMA Internal Medicine* 176(9), 1334–1343.
- Robert Wood Johnson Foundation (2014). 2014 county health rankings and roadmaps. Prepared by Social Explorer. Accessed: 2018-03-27.
- Rosenbaum, P. R. and D. B. Rubin (1983, April). The central role of the propensity score in observational studies for causal effects. *Biometrika* 70(1), 41–55.
- Rubin, D. B. (1974, October). Estimating causal effects of treatments in randomized and nonrandomized studies. *Journal of Educational Psychology* 66(5), 688–701.
- Rubin, D. B. (1980). Randomization Analysis of Experimental Data: The Fisher Randomization Test Comment. *Journal of the American Statistical Association* 75(371), 591–593.
- Schmidhuber, J. (2015). Deep learning in neural networks: An overview. *Neural networks* 61, 85–117.
- Smith, M. T. (1996). The mechanism of benzene-induced leukemia: a hypothesis and speculations on the causes of leukemia. *Environmental Health Perspectives* 104(Suppl 6), 1219.
- Southwest Pennsylvania Environmental Health Project (2015). Summary on compressor stations and health impacts. <http://www.environmentalhealthproject.org/files/Summary%20Compressor-station-emissions-and-health-impacts-02.24.2015.pdf>. Accessed: 2018-03-27.
- Sparapani, R. A., B. R. Logan, R. E. McCulloch, and P. W. Laud (2016). Nonparametric survival analysis using Bayesian additive regression trees (BART). *Statistics in medicine* 35(16), 2741–2753.
- Strobl, C., J. Malley, and G. Tutz (2009). An introduction to recursive partitioning: rationale, application, and characteristics of classification and regression trees, bagging, and random forests. *Psychological methods* 14(4), 323.
- Stuart, E. A. (2010, February). Matching methods for causal inference: A review and a look forward. *Statistical science : a review journal of the Institute of Mathematical Statistics* 25(1), 1–21.
- US Census Bureau (2014). American community survey 2014 (5 year estimates). Prepared by Social Explorer. Accessed: 2018-03-27.
- Wang, C., F. Dominici, G. Parmigiani, and C. M. Zigler (2015). Accounting for uncertainty in confounder and effect modifier selection when estimating average causal effects in generalized linear models. *Biometrics* 71(3), 654–665.
- Westreich, D. and S. R. Cole (2010, March). Invited Commentary: Positivity in Practice. *American Journal of Epidemiology* 171(6), 674–677.
- Westreich, D., J. Lessler, and M. J. Funk (2010). Propensity score estimation: neural networks, support vector machines, decision trees (cart), and meta-classifiers as alternatives to logistic regression. *Journal of clinical epidemiology* 63(8), 826–833.

- Wolf Eagle Environmental (2009). Town of dish, texas ambient air monitoring analysis final report. https://townofdish.com/objects/DISH_-_final_report_revised.pdf. Accessed: 2018-05-08.
- World Trade Center Health Program (2015). Minimum latency & types or categories of cancer. <https://www.cdc.gov/wtc/pdfs/WTCHP-Minimum-Cancer-Latency-PP-01062015.pdf>. Accessed: 2018-03-29.
- Yang, S. and P. Ding (2018). Asymptotic inference of causal effects with observational studies trimmed by the estimated propensity scores. *Biometrika*.
- Zhou, Q. and J. S. Liu (2008). Extracting sequence features to predict protein–dna interactions: a comparative study. *Nucleic acids research* 36(12), 4137–4148.
- Zigler, C., C. Kim, C. Choirat, J. Hansen, Y. Wang, L. Hund, J. Samet, G. King, and F. Dominici (2016). Causal inference methods for estimating long-term health effects of air quality regulations. Research report 187. *Boston, MA: Health Effects Institute*.
- Zigler, C. M. and M. Cefalu (2017). Posterior predictive treatment assignment for estimating causal effects with limited overlap. *arXiv preprint arXiv:1710.08749*.

A Appendix

A.1 BART+SPL MCMC Sampling Scheme for Continuous Outcomes

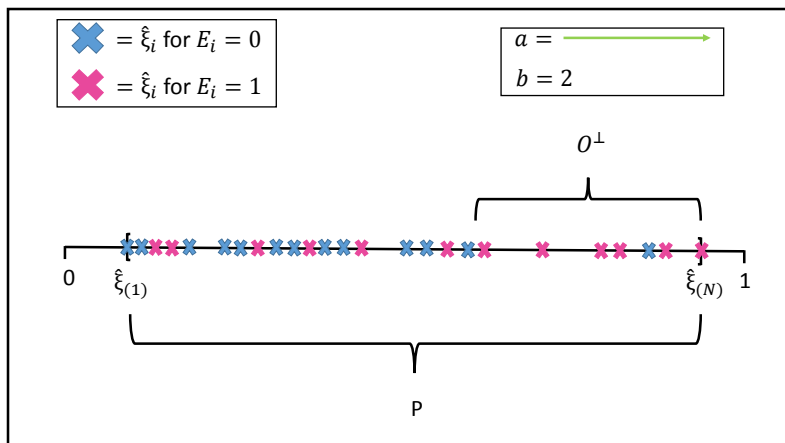
BART+SPL can be implemented via an MCMC sampling scheme that is easily executed in R software (R Core Team, 2016) with the help of the existing dbarts package (Chipman et al., 2010) for drawing samples from a BART. The full conditional distribution of the parameters in a given tree in the BART,

$p(\mathcal{T}_j, \mathcal{M}_j | Y^{obs}, \sigma_B^2, \mathcal{T}_1, \dots, \mathcal{T}_{j-1}, \mathcal{T}_{j+1}, \dots, \mathcal{T}_J, \mathcal{M}_1, \dots, \mathcal{M}_{j-1}, \mathcal{M}_{j+1}, \dots, \mathcal{M}_J)$, depends only on the observed data and the other tree parameters only through the partial residuals $\mathbf{V}_{ji} = Y_i^{obs} - \sum_{l \neq j} g(X_i; \mathcal{T}_l, \mathcal{M}_l)$. Invoking this simplification, BART can be fit using a technique called Bayesian backfitting or backfitting MCMC (Hastie and Tibshirani, 2000), where the MCMC samples from a given tree are drawn while treating the parameters from all other trees as constant. We outline the steps for obtaining MCMC samples from BART+SPL below, assuming the default BART prior distributions recommended in Chipman et al. (2010) and non-informative Normal-Inverse Gamma priors for the spline model. This sampling scheme assumes that only one smoothing stage model is fit, i.e., the RN contains observations from only one exposure group; however, if the RN contains observations from both exposure groups and two splines are needed, steps (5) and (6) can easily be repeated for a second spline model. We assume that each of the BART and spline parameters has been initialized, so that we begin with $\{\mathcal{T}_j^{(0)}, \mathcal{M}_j^{(0)}, \sigma_B^2^{(0)}, \beta^{(0)}, \sigma_S^2^{(0)}\}$.

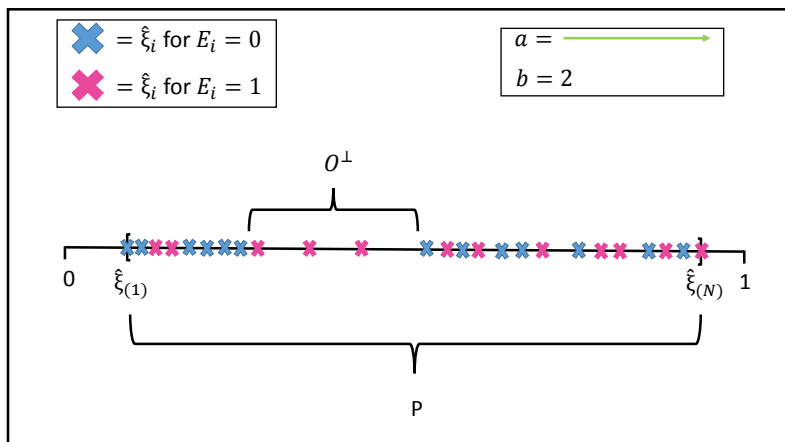
For $m = 1, \dots, M$,

1. For tree j , ($j = 1, \dots, J$)
 - (a) Draw $\mathcal{T}_j^{(m)}$ from $p(\mathcal{T}_j | \mathbf{V}_j^{(m-1)}, \sigma_B^2^{(m-1)})$ using the Metropolis Hastings algorithm described by Chipman et al. (1998)
 - (b) Draw $\mathcal{M}_j^{(m)}$ from $p(\mathcal{M}_j | \mathbf{V}_j^{(m-1)}, \sigma_B^2^{(m-1)}, \mathcal{T}_j^{(m)})$ through a random sample from the Normal distribution
2. Draw $\sigma_B^2^{(m)}$ from $p(\sigma_B^2 | Y_O^{obs}, \mathcal{T}_1^{(m)}, \dots, \mathcal{T}_J^{(m)}, \mathcal{M}_1^{(m)}, \dots, \mathcal{M}_J^{(m)})$ through a random sample from an Inverse-Gamma distribution
3. Draw $Y_O^{mis(m)}$ from $p(Y_O^{mis} | Y_O^{obs}, \mathcal{T}_1^{(m)}, \dots, \mathcal{T}_J^{(m)}, \mathcal{M}_1^{(m)}, \dots, \mathcal{M}_J^{(m)}, \sigma_B^2^{(m)})$ through a random sample from a Normal distribution
4. Form $\Delta_O^{(m)}$ as the appropriate linear combination of Y_O^{obs} and $Y_O^{mis(m)}$, per Equation 2.
5. Draw $\beta^{(m)}$ from $p(\beta | \Delta_O^{(m)}, \sigma_S^2(m-1))$ through a random sample from the Normal distribution
6. Draw $\sigma_S^2^{(m)}$ from $p(\sigma_S^2 | \Delta_O^{(m)}, \beta^{(m)})$ through a random sample from an Inverse-Gamma distribution
7. Draw $\Delta_{O\perp}^{(m)}$ from $p(\Delta_{O\perp} | \Delta_O^{(m)}, \beta^{(m)}, \sigma_S^2^{(m)}, \tau_{Oq})$ through a random sample from a Normal distribution
8. Draw $\Delta_P^{(m)}$ by executing B iterations of the Bayesian bootstrap on $\{\tilde{\Delta}_O^{(m)}, \tilde{\Delta}_{O\perp}^{(m)}\}$ and randomly selecting one of the B bootstrap sample averages.

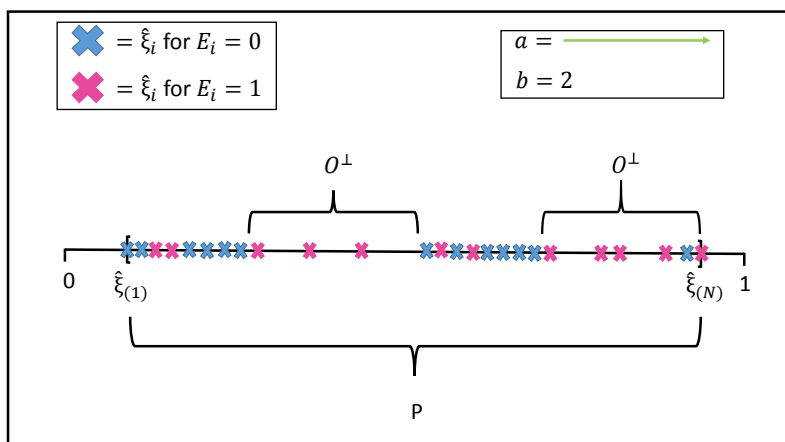
A.2 Supplementary Tables and Figures



(a)

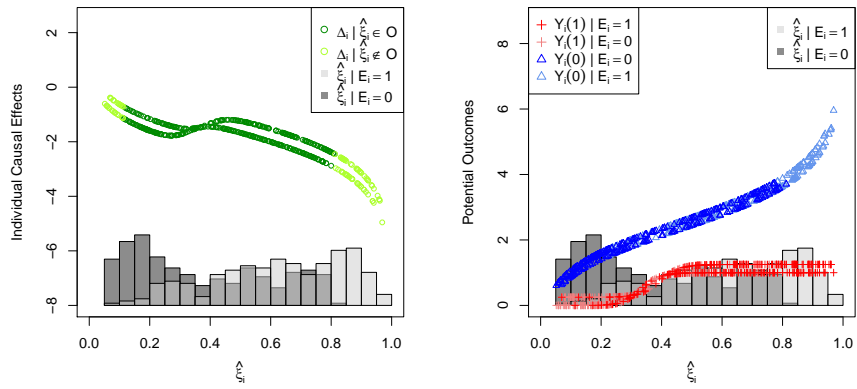


(b)

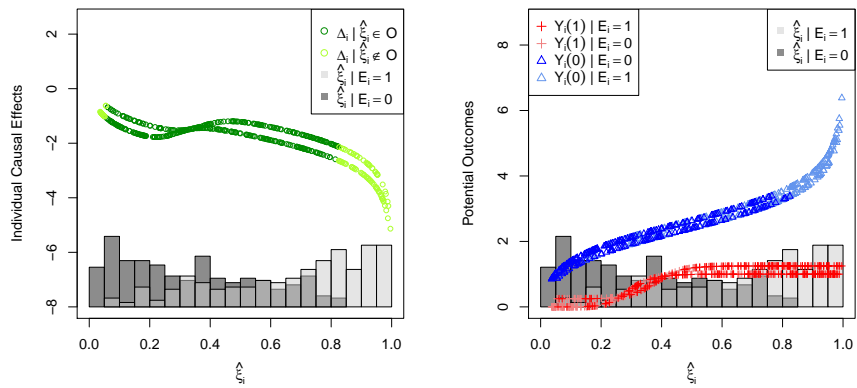


(c)

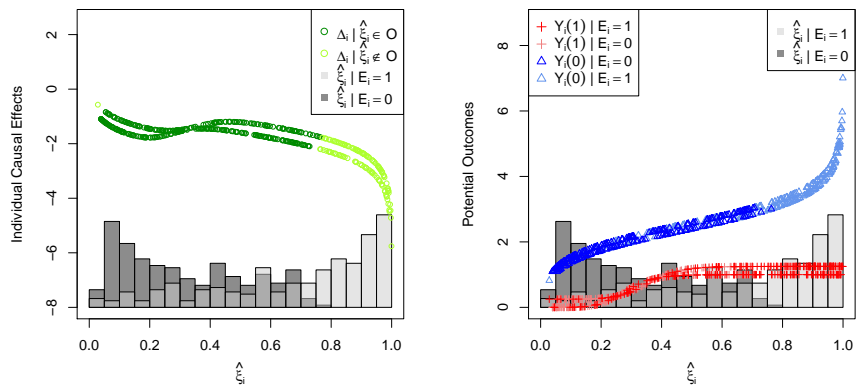
Figure 2: Examples of several types of propensity score non-overlap regions that can be captured by our definition. (a) demonstrates non-overlap in the tail of the distribution, (b) demonstrates non-overlap in the interior of the distribution, and (c) demonstrates multiple intervals of non-overlap.



(a)



(b)



(c)

Figure 3: Examples of the three simulation scenarios described in Section 3.1: simulation 3.1A (a), simulation 3.1B (b), and simulation 3.1C (c).

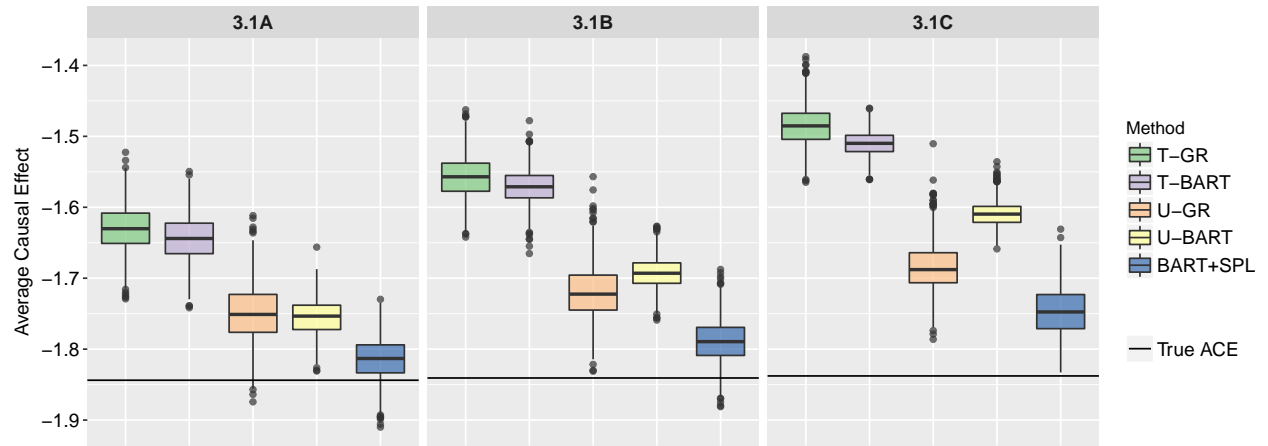
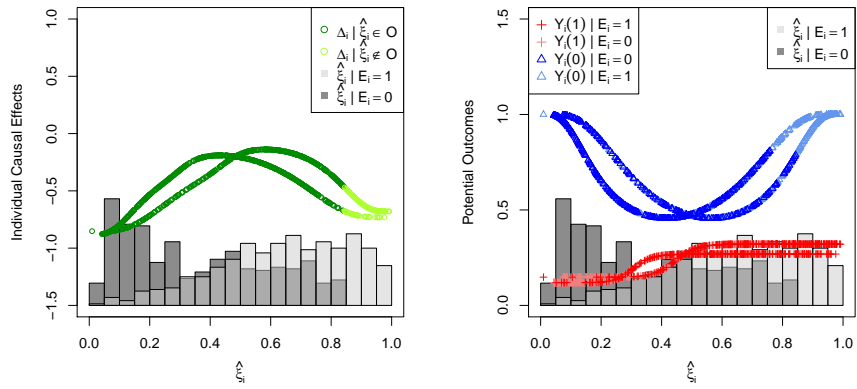
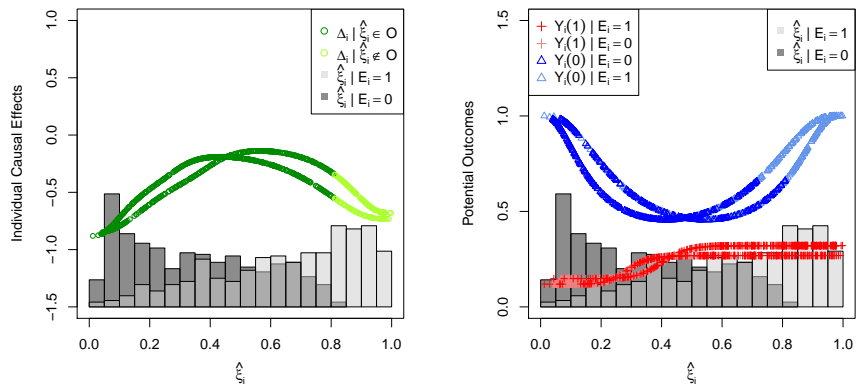


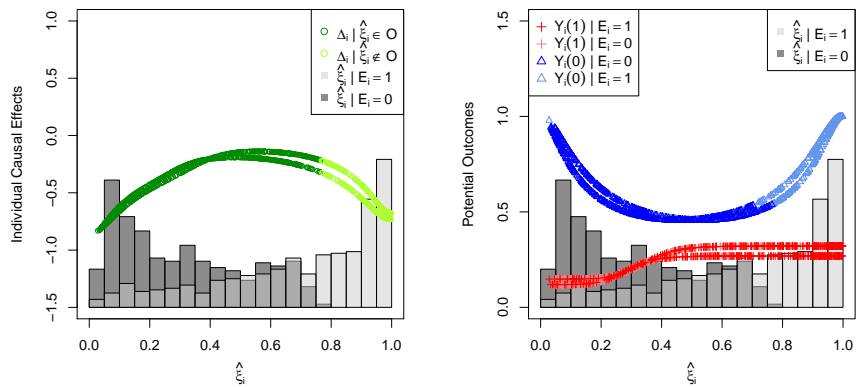
Figure 4: Estimates of Average Causal Effects from simulations in Section 3.1



(a)



(b)



(c)

Figure 5: Examples of the three simulation scenarios described in Section 3.2: simulation 3.2A (a), simulation 3.2B (b), and simulation 3.2C (c).

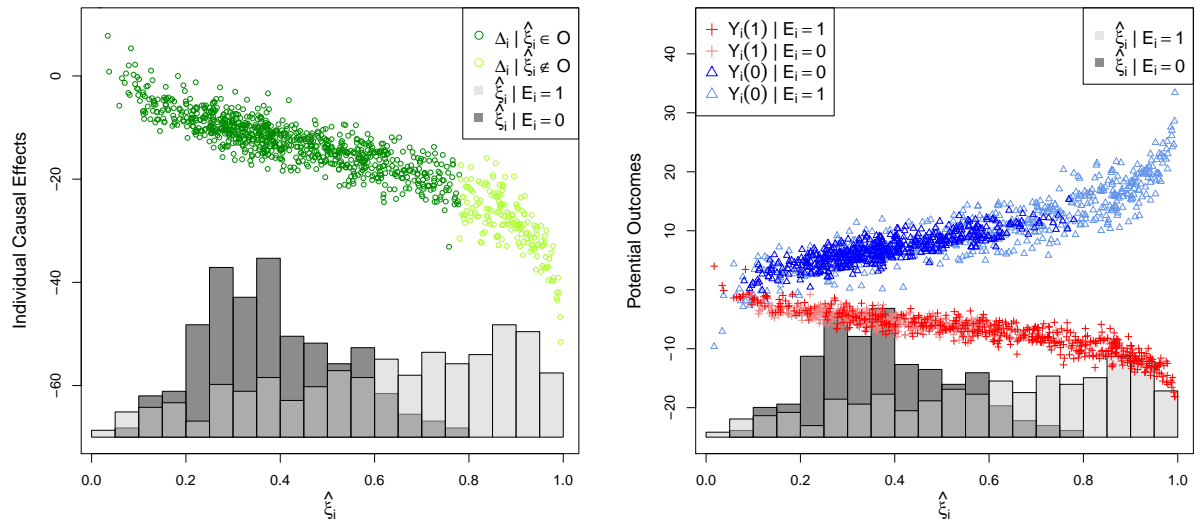
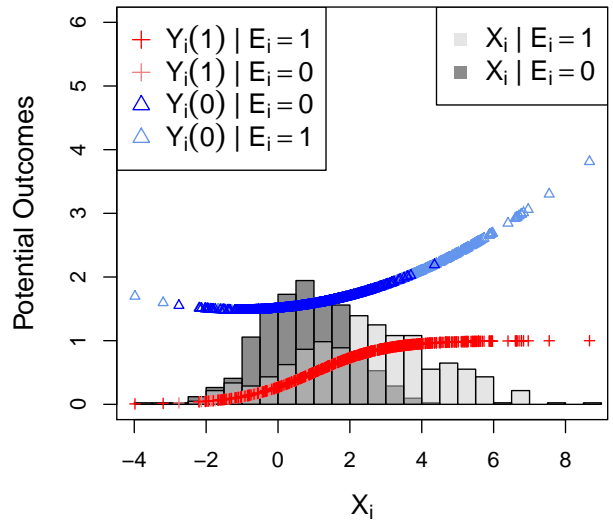
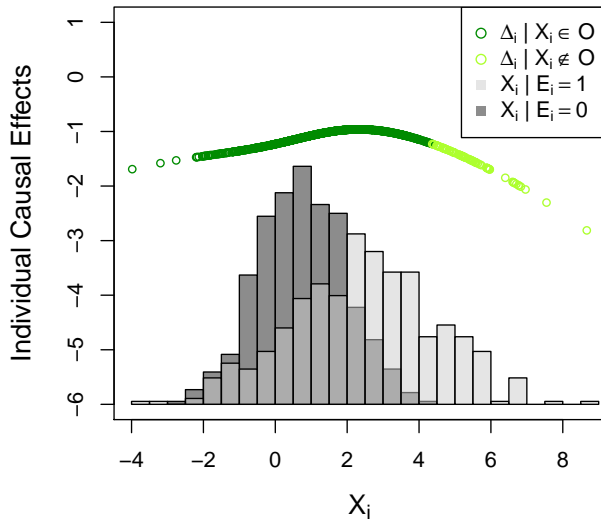
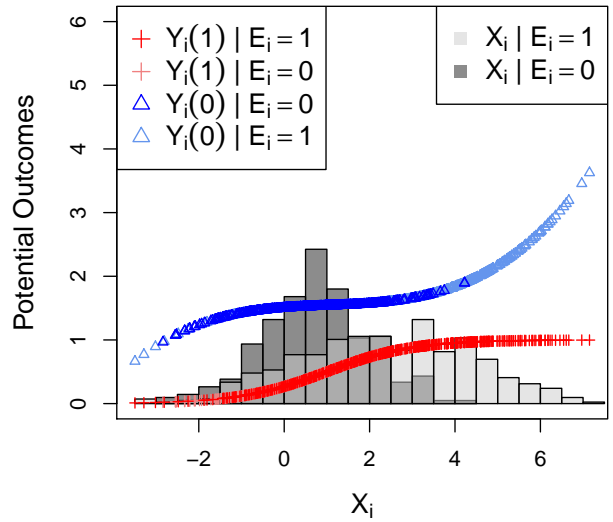
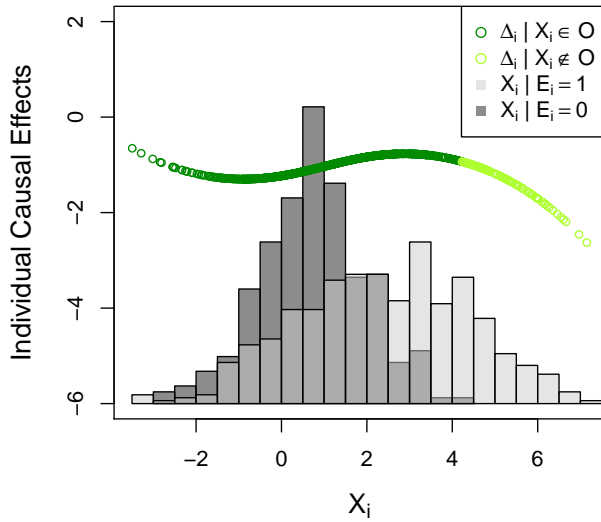


Figure 6: Example simulated dataset from Section 3.3 with $p = 20$, i.e., 10 true confounders and 10 randomly generated predictors.



(a)



(b)

Figure 7: Example datasets from simulation 3.4A (a) and simulation 3.4B (b) in Section 3.4.

Table 7: Summary of outcome and confounder variables overall and stratified by exposure status. All rates are per 100,000 population.

Variable	Total (N=978)		Unexposed (N=687)		Exposed (N=291)	
	Mean	SD	Mean	SD	Mean	SD
2014 Thyroid Rate	0.55	0.06	0.55	0.06	0.56	0.05
Change Thyroid Rate 1980-2014	1.71	8.03	1.16	7.67	2.99	8.71
2014 Leukemia Rate	9.64	0.90	9.66	0.90	9.6	0.89
Change Leukemia Rate 1980-2014	-4.29	8.54	-4.26	8.24	-4.36	9.21
Rate of Primary Care Physicians	801.39	1330.09	773.65	1398.35	866.87	1152.66
Percent Uninsured	17.74	5.53	17.36	5.48	18.64	5.55
Percent Diabetic	83.02	8.14	83.33	8.07	82.29	8.29
Percent Current Smokers	20.51	6.17	20.33	6.49	20.95	5.33
Percent Healthy Food Access	10.18	8.19	10.33	8.67	9.82	6.95
Percent Obese	28.43	5.19	28.45	5.25	28.40	5.05
Food Environment Index	7.31	1.32	7.33	1.32	7.27	1.30
Population Density	99.38	332.66	106.05	372.07	83.62	212.12
Percent Male	50.10	1.89	50.10	1.83	50.11	2.05
Percent <55	69.61	6.17	68.88	6.46	71.36	5.01
Percent White	84.88	16.39	86.16	15.77	81.86	17.42
Average Household Size	2.50	0.25	2.47	0.25	2.56	0.26
Percent \geq Bachelors Degree	20.01	7.80	20.36	8.19	19.19	6.74
Percent Unemployed	7.00	3.69	6.80	3.60	7.48	3.84
Median Household Income	46296	10436	46100	10489	46759	10314
Gini Index of Inequality	0.44	0.03	0.44	0.03	0.44	0.04
Percent Own Home	71.85	7.44	72.00	7.63	71.48	6.97
Median Rent, Proportion Income	27.43	4.43	27.28	4.41	27.76	4.45
Average Commute Time	21.28	5.30	21.08	5.34	21.75	5.19